Tran-SET

Transportation Consortium of South-Central States

Solving Emerging Transportation Resiliency, Sustainability, and Economic Challenges through the Use of Innovative Materials and Construction Methods: From Research to Implementation

Multifunctional corrosion control system as a sustainable approach for reinforced concrete elements

Project No. 20CTAMU22

Lead University: Texas A&M University

Final Report

September 2021

Disclaimer

The contents of this report reflect the views of the authors, who are responsible for the facts and the accuracy of the information presented herein. This document is disseminated in the interest of information exchange. The report is funded, partially or entirely, by a grant from the U.S. Department of Transportation's University Transportation Centers Program. However, the U.S. Government assumes no liability for the contents or use thereof.

Acknowledgements

The authors would like to acknowledge the financial support for this study by the Transportation Consortium of South-Central States (Tran-SET).

TECHNICAL DOCUMENTATION PAGE

1. Project No.	2. Government Accession No.	3. Recipient's Catalog No.
20CTAMU22		

4. Title and Subtitle	5. Report Date
Multifunctional corrosion control system as a sustainable approach for reinforced concrete elements	Sept. 2021
	6. Performing Organization Code

7. Author(s)	8. Performing Organization Report No.
PI: Homero Castaneda-Lopez https://orcid.org/0000-0002-9252-7744 Co-PI: Miladin Radovic https://orcid.org/0000-0003-4571-2848 Co-PI: Brendy Rincon https://orcid.org/0000-0002-8895-1016 Co-PI: Oladis Troconis https://orcid.org/0000-0002-3693-5057 Co-PI : Arturo Montoya https://orcid.org/ 0000-0003-1429-5105 GRA: Changkyu Kim https://orcid.org/0000-0002-9050-6309 GRA: Loreto Dacio https://orcid.org/0000-0002-2186-9835	

9. Performing Organization Name and Address	10. Work Unit No. (TRAIS)
Transportation Consortium of South-Central States (Tran-SET) University Transportation Center for Region 6 3319 Patrick F. Taylor Hall, Louisiana State University, Baton Rouge, LA 70803	**11. Contract or Grant No.** 69A3551747106

12. Sponsoring Agency Name and Address	13. Type of Report and Period Covered
United States of America Department of Transportation Research and Innovative Technology Administration	Final Research Report Aug. 2020 – Sep. 2021
	14. Sponsoring Agency Code

15. Supplementary Notes

Report uploaded and accessible at Tran-SET's website (http://transet.lsu.edu/).

16. Abstract

Corrosion inhibitors can be utilized to decrease the corrosion kinetics and therefore increase the durability of reinforced concrete structures. Recently, a green synthesized organic compound, 1-benzyl-4-phenyl-1H-1,2,3-triazole (BPT), was shown to be a successful green organic corrosion inhibitor for mild steel. Studies suggested that the BPT adsorbs chemically onto the steel and acts as a mixed inhibitor, suppressing both the anodic and cathodic corrosion kinetics of steel. In addition, microcapsules have shown to be an efficient way for a controlled inhibitor release in reinforced concrete structures. On the other hand, geopolymers (GPs) comprised of a long range of covalently bonded alumino-silicates, with amorphous network structure are generally considered as a suitable substitute for OPC for many structural applications due to their high strength and durability. The use of recycled waste materials or natural abundant materials for the production of GPs has attracted world-wide attention as it presents an environment-friendly aspect that may shed light on for replacing traditional OPC by its sustainability. One of the advantages of GPs is the significant reduction to CO_2 emission due to the energy consumption, the geopolymers utilize materials such as fly-ash, which is a byproduct of coal combustion, or natural precursor materials (clays, basalt rocks, etc.) and their derives (metakaolin), which does not produce net CO_2 emission. Recent studies have shown that GPs based cements can hinder the corrosion of reinforcement steel in concrete structures when compared to OPC, mostly because of lower chloride ingress (due to barrier protective capabilities) and the highly alkaline pH nature of geopolymer cements.

17. Key Words	18. Distribution Statement
Geopolymer, Reinforced Concrete, Inhibitors, Corrosion	No restrictions. This document is available through the National Technical Information Service, Springfield, VA 22161.

19. Security Classif. (of this report)	20. Security Classif. (of this page)	21. No. of Pages	22. Price
Unclassified	Unclassified	41	

Form DOT F 1700.7 (8-72) **Reproduction of completed page authorized.**

SI* (MODERN METRIC) CONVERSION FACTORS

APPROXIMATE CONVERSIONS TO SI UNITS

Symbol	When You Know	Multiply By	To Find	Symbol
		LENGTH		
in	inches	25.4	millimeters	mm
ft	feet	0.305	meters	m
yd	yards	0.914	meters	m
mi	miles	1.61	kilometers	km
		AREA		
in^2	square inches	645.2	square millimeters	mm^2
ft^2	square feet	0.093	square meters	m^2
yd^2	square yard	0.836	square meters	m^2
ac	acres	0.405	hectares	ha
mi^2	square miles	2.59	square kilometers	km^2
		VOLUME		
fl oz	fluid ounces	29.57	milliliters	mL
gal	gallons	3.785	liters	L
ft^3	cubic feet	0.028	cubic meters	m^3
yd^3	cubic yards	0.765	cubic meters	m^3
		NOTE: volumes greater than 1000 L shall be shown in m^3		
		MASS		
oz	ounces	28.35	grams	g
lb	pounds	0.454	kilograms	kg
T	short tons (2000 lb)	0.907	megagrams (or "metric ton")	Mg (or "t")
		TEMPERATURE (exact degrees)		
^oF	Fahrenheit	5 (F-32)/9 or (F-32)/1.8	Celsius	^oC
		ILLUMINATION		
fc	foot-candles	10.76	lux	lx
fl	foot-Lamberts	3.426	candela/m^2	cd/m^2
		FORCE and PRESSURE or STRESS		
lbf	poundforce	4.45	newtons	N
lbf/in^2	poundforce per square inch	6.89	kilopascals	kPa

APPROXIMATE CONVERSIONS FROM SI UNITS

Symbol	When You Know	Multiply By	To Find	Symbol
		LENGTH		
mm	millimeters	0.039	inches	in
m	meters	3.28	feet	ft
m	meters	1.09	yards	yd
km	kilometers	0.621	miles	mi
		AREA		
mm^2	square millimeters	0.0016	square inches	in^2
m^2	square meters	10.764	square feet	ft^2
m^2	square meters	1.195	square yards	yd^2
ha	hectares	2.47	acres	ac
km^2	square kilometers	0.386	square miles	mi^2
		VOLUME		
mL	milliliters	0.034	fluid ounces	fl oz
L	liters	0.264	gallons	gal
m^3	cubic meters	35.314	cubic feet	ft^3
m^3	cubic meters	1.307	cubic yards	yd^3
		MASS		
g	grams	0.035	ounces	oz
kg	kilograms	2.202	pounds	lb
Mg (or "t")	megagrams (or "metric ton")	1.103	short tons (2000 lb)	T
		TEMPERATURE (exact degrees)		
^oC	Celsius	1.8C+32	Fahrenheit	^oF
		ILLUMINATION		
lx	lux	0.0929	foot-candles	fc
cd/m^2	candela/m^2	0.2919	foot-Lamberts	fl
		FORCE and PRESSURE or STRESS		
N	newtons	0.225	poundforce	lbf
kPa	kilopascals	0.145	poundforce per square inch	lbf/in^2

TABLE OF CONTENTS

LIST OF FIGURES

LIST OF TABLES

ACRONYMS, ABBREVIATIONS, AND SYMBOLS

Al	Aluminum
C_{be}	Bulk-Electrode Capacitance
C_c	Concrete Bulk Pore Capacitance
C_{dl}	Double-Layer Capacitance
CE	Counter Electrode
Cl	Chlorine/Chloride ion
CPE	Constant Phase Element
EEC	Electrical Equivalent Circuit
EIS	Electrochemical Impedance Spectroscopy
GPs	Geopolymers
K	Potassium
K-GP	Potassium-based Geopolymer
MK	Metakaolin
NaCl	Sodium Chloride
OCP	Open Circuit Potential
OPC	Ordinary Portland Cement
R_{be}	Bulk-Electrode Resistance
R_c	Concrete Bulk Resistance
R_{ct}	Charge-Transfer Resistance
R_s	Solution Resistance
RC	Reinforced Concrete
RE	Reference Electrode
SCE	Saturated Calomel Electrode
Si	Silicon
WE	Working Electrode

EXECUTIVE SUMMARY

In order to improve the durability of the transportation infrastructure affected by corrosion in the most efficient manner, we proposed to characterize and develop a new material to manage corrosion in reinforced concrete (RC) elements. The desirable features of this propose material system would include the barrier effect to the corrosion precursors and harsh environment hindering the RC elements with time.

Reinforced Concrete (RC) structures are vital to the US' infrastructure due to their high durability and superior mechanical performance when used as prime materials for bridges, superstructures and other civil engineering applications. Despite of such importance, the RC elements have been deteriorated rapidly when exposed to corrosive environments. The deterioration mechanism is known to follow the evolution concept under steady state conditions including three different stages: I) mass transport of the ionic corrosive precursors (chlorides) within the concrete matrix, II) activation of the metallic rebar due to a loss of native passive layer, and III) increase charge transfer reaction rate of the rebar which leads to corrosion products at the rebar and possible concrete cracking. This could be the cause of the current inadequate performance levels we are encountering in our infrastructure elements in region 6.

Corrosion inhibitors can be utilized to decrease the corrosion kinetics and therefore increase the durability of reinforced concrete structures. Recently, a green synthesized organic compound, 1-benzyl-4-phenyl-1H-1,2,3-triazole (BPT), was shown to be a successful green organic corrosion inhibitor for mild steel. Studies suggested that the BPT adsorbs chemically onto the steel and acts as a mixed inhibitor, suppressing both the anodic and cathodic corrosion kinetics of steel. In addition, microcapsules have shown to be an efficient way for a controlled inhibitor release in reinforced concrete structures. On the other hand, geopolymers (GPs) comprised of a long range of covalently bonded alumino-silicates, with amorphous network structure are generally considered as a suitable substitute for OPC for many structural applications due to their high strength and durability. The use of recycled waste materials or natural abundant materials for the production of GPs have attracted world-wide attention as it presents an environment-friendly aspect that may shed light on for replacing traditional OPC by its sustainability. One of the advantages of GPs is the significant reduce to CO_2 emission due to the energy consumption, the geopolymers utilize materials such as fly-ash, which is a byproduct of coal combustion, or natural precursor materials (clays, basalt rocks, etc.) and their derives (metakaolin), which does not produce net CO_2 emission. Recent studies have shown that GPs based cements can hinder the corrosion of reinforcement steel in concrete structures when compared to OPC, mostly because of lower chloride ingress (due to barrier protective capabilities) and the highly alkaline pH nature of geopolymer cements.

The expected deliverable from this project is a technical report summarizing all tasks and findings including necessary design guidelines of durable reinforced GPC concrete structures. The team also anticipates publishing high-impact research publications including journal and conference articles.

1. INTRODUCTION

Corrosion inhibitors can be utilized to decrease the corrosion kinetics and therefore increase the durability of reinforced concrete metallic materials. Inhibitors are widely used in corrosion technology, but their use as control action for steel corrosion in concrete has been limited. Different studies that have been suggesting the positive effect of different inhibitors applied to reinforced concrete system, but several disadvantages of applying such technology have been noticed. Some of them include the release of some chemicals to the environment resulting in environmental contamination, or the negative influence of the reinforced concrete physico-chemical properties *(1, 2),* and others can lead to health conditions as for the case of calcium nitrite compounds (*3*).

Among different inhibiting substances evaluated that are appropriate for the alkaline medium in concrete, calcium nitrite has provided successful results, even for cracked concrete [4]. Therefore, it has been used commercially with some relative success. However, some disadvantages and issues for this chemical due to carcinogenic and toxic properties have been raised [3], also the cost and scarcity in some countries for related compounds. Other routes have been taken to overcome the previous issues, some additives have been studied in an effort to use a more sustainable replacement by eliminating or decreasing the use of calcium nitrite. It has been found that $Ca(NO_2)_2$ improves the corrosion resistance of steel to chloride-ion attacks for w/c ratios lower than 0.5. Troconis de Rincon et.al. *(2, 5-8),* studied the use of ZnO and its mixture with $Ca(NO_2)_2$.

It was found that when using 2%wt $Ca(NO_2)_2$ the metal lost its passivity following 400 days of exposure (*8)*. But, when ZnO was added, at equal proportions, the steel remained in its passive state, reducing Cl- diffusion to the reinforcement, which allows $Ca(NO_2)_2$ to act efficiently on the reinforcement by maintaining its passivity [9]. The best results were found when equal proportions of the two inhibitors were used (ZnO/$Ca(NO_2)_2$ at 2%wt. Different approaches, have been targeting for nitrite replacement *(10)* by using different compounds (gluconate, phosphate, urotropine, chromates, resorcinol, fluoroglucinol, and zinc oxide) with not success.

Other investigations *(11)* developed rehabilitation processes for reinforced concrete structures by using four inhibitor formulations: (i) organic inhibitor; (ii) mixture of surfactant and amino salts in water, or volatile corrosion inhibitor; (iii) alcanolamine additive; and (iv) $Ca(NO_2)_2$. The four inhibitors were applied in presence of chloride-contaminated concrete and pre-corroded reinforcements, the results indicated that the use of (ii) and (iii) resulted in a significant reduction in corrosion rate, contrary the others (i) and (iv) produced a substantial increase in corrosion.

More recently, Sousa Rivetti M et al. *(12)* and Han-Seung Lee et. al. *(13)* published a review on the recent trends in corrosion inhibitors for reinforced concrete and their application in the laboratory and field conditions. They found that there are several organic and inorganic inhibitors available to control the corrosion of the steel rebar, however most of them are synthetic in nature and are prone to release environmentally hazard chemicals.

Geopolymers as “a class of totally inorganic, alumino-silicate based ceramics that are charge balanced by group I oxides. They are rigid gels, which are made under relatively ambient temperature and pressure into net shape bodies” *(14)*. In the last 40 years, Geopolymers have been extensively studied as cementitious materials for concrete structures and soil stabilization *(15-17),* fire resistant and thermal insulating coatings *(18, 19),* materials for encapsulation of radioactive

waste *(20)*, and corrosion resistant coatings and adhesives *(21-23)*, etc. The chemistry of geopolymers can described with chemical formula $M_n[-(SiO_2)_z - AlO_2-]_n \cdot wH_2O$ where M is the alkali metal cation, n is the degree of polymerization, z is the Si/Al ratio (usually 1, 2, 3…), and w is the molar water quantity. It is worth noting here, that the activating metal cation M (usually Na^+, K^+,etc.) is believed to stay in the geopolymer framework cavities close to Al and balance the negative charge of the IV-coordinated [-AlO_2-]- *(21)*. Geopolymers are usually prepared with a Si/Al ratio of 1.8-2.2, an $H_2O/(Al_2O_3 + SiO_2)$ ratio of 2.0-5.0, and a M/Al ratio of 0.9-1.2 (where M is Na or K).

Tran-SET **project No. 19CTAM02** has been focused on developing environment friendly geopolymers as a cementitious material for reinforced concrete to increase the durability of RC structures. The project includes the study of reinforced GP concrete samples exposed to the corrosive conditions at laboratory scale. This study revels fundamental mechanism(s) of rebar corrosion in reinforced GP concrete and understanding of the role that GPs have on in corrosion control. The results of current and previous research will provide enormous leverage for a more efficient corrosion management system based on corrosion mechanisms and control conditions.

2. OBJECTIVES

The main objective of this study is to develop an innovative, sustainable, and eco-friendly multifunctional corrosion control technology, based on geo-polymer binders with BPT (a green synthesized organic compound) additions that will have a simultaneous dual action. That is to provide a barrier to corrosion species, while inhibiting the corrosion of the reinforcing steel. It is expected that this research project will contribute to the infrastructure integrity, durability and sustainability by implementing a new sustainable multifunctional corrosion control system to the concrete field to achieve high corrosion resistance and enhanced durability with alleviated environmental contamination.

More specific objectives of the proposed projects are:

- Conduct electrochemical testing of either BPT, GPC or a combination of both control actions concrete reinforced with steel rebar in simulated corrosive environment using both AC and DC methods.
- Determine corrosion mechanism and kinetics of the reinforcement steel in BPT integrated in concrete.
- Optimize the corrosion control action composition for maximum corrosion protection of reinforcing steel rebar.

3. LITERATURE REVIEW

3.1. Geopolymer-based Cement Concrete

Geopolymer concrete (GPC) has been of interest since the early 2000s and achieved strength that is on par with OPC concrete *(22-24)*. However, as of 2016, most of the studies focuses on optimizing FA-based GPC concrete while curing them under elevated temperature, which is not ideal for implementation *(25)*. The main shortcoming with studies that utilize FA is that FA does not have a consistent composition and it can vary a lot depending on the location that it is sourced from. This means that it is usually difficult to reproduce the studies, in addition, the price of FA has been surging lately with the increase in demand from the concrete industry and the shift of energy production from coal plants. MK-based GPC has been more extensively studied in the past few decades for a more fundamental understanding on GPC since it is a pure aluminosilicate source that is reactive and more consistent regardless of the source. Some of the examples are physical evolution with temperature *(26-28)*, formation of crystalline phase [29,30], structural studies using nuclear magnetic resonance (NMR) spectroscopy *(31)*. However, there are only a few studies on mechanical properties and long-term durability *(32-38)*. One of the main issues with the durability of concrete structure is the corrosion of steel rebar reinforcement, which is an extensive field of interest in the OPC community *(39)*, but not a lot of research has been done for reinforced GPC concrete. Many researchers have claimed GPC to be better than OPC when it comes to inhibiting corrosion *(40,41)*, however, there are only about half a dozen of papers available in the public domain, and they have conflicting conclusions on the corrosion inhibiting performance of GPC *(42-48)*. One of the main reasons for the conflicting results is because all of the research except for part of one use FA, and as mentioned before, FA can produce different results due to varied composition from different sources. Another issue that makes it difficult to compare between the studies is that all the conclusions were drawn without any sort of systematic parametric testing, in order words, none of the studies provide any guidance towards producing better GP to inhibit rebar corrosion. Instead, the studies synthesized a couple of GP compositions and draws the conclusion from there. The rest of the section will do an in-depth review on the available literature that investigated the chloride-induced corrosion inhibiting performance of GPC in chronological order.

Miranda et al. *(42)* is one of the earliest study on the chloride-induced corrosion resistant performance of GPC. Miranda et al. compared OPC mortar with two types of FA-based GPC mortars where one was activated with sodium hydroxide while the other was activated with a mixture of sodium hydroxide and sodium silicate. The samples were cured in elevated temperature and designed in a way that there's a 7 mm penetration depth between the surface and the steel rebar, but the detailed condition on the corrosive environment were not reported in the paper. Through electrochemical measurements, it was shown in the study that FA-based GPC achieves a better early protection than OPC, but the degree of protection decreases gradually for FA-based GPC while it improves for OPC during the 3-month testing period. This is most likely because fresh GPC paste already has a high pH because of the activating solution, while OPC becomes more alkaline with time as more and more of the components dissolve. Overall, this study showed that FA-based GPC is not as effective as OPC to protect steel rebar from chloride-induced corrosion in the long term.

Reddy et al. *(43)* compared OPC concrete with two types of FA-based GPC concrete, where one was synthesized with 8M sodium hydroxide-sodium silicate blend while the other was synthesized with 14M sodium hydroxide-sodium silicate blend. The OPC concrete specimens were cured in ambient condition while the GPC concrete specimens were cured in elevated condition. The specimens partially immersed in seawater solution for 21 days before testing, then a DC current is applied to accelerate the corrosion. This study clearly showed that GPC concrete is vastly superior over OPC concrete with corrosion current measurement and weight loss measurement of the rebar. Particularly for the weight loss measurement of rebar, the 3 rebars in OPC loss between 50-75% of the weight while all 6 rebars in GPC showed no significant weight loss. Even though GPC showed significantly better performance over OPC, the result should still be taken with a grain of salt since GPC specimens are cured under elevated conditions while OPC specimens weren't. Another factor that could have affected the study is the difference in water content and superplasticizer between GPC and OPC specimens since the GPC specimens had superplasticizer and significantly less water than the OPC specimens.

In Shaikh's work *(44)*, 7 mixes were made with OPC as the control mix and the rest are GPC with either 14M or 16M NaOH and ratio of sodium silicate to sodium hydroxide between 2.5-3.5. The samples were made so that there is a 42 mm of penetration depth from the surface to the rebar. The concrete samples were subjected to 8 wet/dry cycles with 4 days in 3.5 wt% sodium chloride solution and 3 days of drying. Shaikh reported that GPC samples overall performed better than OPC samples in terms of rebar mass loss, chloride penetration, and open-circuit potential (OCP). From the mass loss measurement, it was observed that OPC did not have good adhesion to rebar while GPC did, and the rebars in OPC loss about 0.5% of mass while no significant mass loss can be measured from rebars in GPC samples. It was also observed from chloride penetration and OCP test that GPC with higher concentrated sodium hydroxide and more sodium silicate performed better. A potential explanation for these results is that the more concentrated sodium hydroxide solution is able to dissolve the FA better and higher content of sodium silicate provides more dissolved silica for geopolymerization.

Chindaprasirt et al. *(45)* prepared 6 different mixes of GPC using varied concentration of sodium hydroxide ranging from 8 to 18M with class C FA. The samples were made so that there's a 94 mm of penetration depth between the surface and the rebar. The samples are cured for 28 days in ambient condition and then exposed to marine environment for 3 years. The study shows that the FA-based GPC can effectively inhibit the diffusion of chloride ions when the activator solution (sodium hydroxide) is more than 14M. The weight loss measurement of rebar also observes the same result from the chloride diffusion test. This study showed that class C FA-based GPC concrete in real marine environment has some promising potentials, however, it did not show how OPC would perform under the same condition. In addition, the parametric test done in this study simply showed that well-reacted GPC can inhibit the diffusion of chloride better and does not provide any further insights.

Babaee et al. *(46)* investigated the performance of 1 GPC composition using a blend of FA, ultra-fine FA, and ground granulated blast-furnace slag activated by a mixture of 12M sodium hydroxide and sodium silicate. The samples are made so that there's a penetration depth of 73 mm, and then cured under elevated temperature. For testing, the samples are subjected to 1 week of immersion in 3.5 wt% sodium chloride solution, then exposed to ambient condition for 2 weeks for a total of 11 cycles. From OCP and linear polarization resistance measurements, it was found that the GPC samples has comparable performance with the results on OPC from one of their previous studies

(49). This study has done a very thorough investigation on the chloride-induced corrosion performance of GPC, the only shortcoming would be the lack parametric study and the usage of local materials, which does not give much guidance to other researchers who would want to further the study.

Tennakoon et al. *(47)* compared OPC with 3 different mixes of GPC that used different FA to slag ratios. The FA and slag are activated with sodium silicate, and the samples are cured in ambient condition for 28 days. The samples were prepared so that there's a penetration depth of 465 mm, and then they were immersed in either 2.83M (16.5 wt%) or 0.6M (3.5 wt%) NaCl solutions. From OCP measurements alone, GPC seems to be inferior when compared to OPC, however, GPC showed better results when looking chloride penetration and visual inspection of the corrosion product on the rebar. Between the 3 GPC compositions, the composition with more slag outperforms the ones with less slag. Overall, this study showed some very interesting results, and the disconnect between electrochemical results and corrosion activity would need further investigations.

Gunasekara et al. *(48)* compared OPC with GPC made from 3 different FAs. The FAs were activated with a mixture of 15M sodium hydroxide and sodium silicate. The samples were made so that there's a 70 mm penetration depth and then cured in elevated temperature condition. After curing, the samples are exposed to 3% sodium chloride solution for a week then ambient condition for 2 weeks, and the cycled for 540 days. Overall, GPC shows similar performance compared to OPC unless chloride is added into the concrete mix, then in that case OPC outperforms GPC significantly. This study also showed that different FA can have significantly varied performance, depending on its composition and reactivity.

3.2. BPT and Inhibitors

Admixtures can be added to concrete to modify many of the material properties of concrete to make it more workable, allow it to set faster and reach full-strength sooner *(50)*. Certain types of admixtures can be added to the concrete mix that can prevent or inhibit corrosion of the embedded reinforcement. These admixtures are known as corrosion inhibitors and they can be classified as either organic or inorganic, as well as anodic, cathodic, or mixed where the inhibitor suppresses both the anodic and cathodic reactions. An inhibitor may reduce corrosion in reinforced concrete by reacting with the chlorides and reducing the ingress of the ions or raising the threshold needed to break the passivation layer, or by reducing the corrosion rate once initiated *(51)*. Some inorganic anodic inhibitors perform this by self-passivating, while some cathodic inhibitors form protective surface deposits *(52)*. Organic inhibitors work to inhibit corrosion by chemisorption onto the surface of the metal, which then promotes growth and maintenance of the intrinsic passive film.

As of now, the only corrosion inhibitor commercially used in reinforced concrete is calcium nitrite ($Ca(NO_2)_2$) and has been reported to have relative success in inhibiting corrosion *(51,53)*. $Ca(NO_2)_2$ is classified as an anodic inhibitor and is typically added to the cement mix as calcium salt. The inhibitor reacts with Cl^-, reducing the chloride concentration and releasing nitrite ions (NO_2). The NO_2 then oxidizes the Fe^{++} ions to produce Fe^{3+} ions, which will precipitate in the concrete and on the steel surface aiding in the passivation of the rebar. This effect has been noted to only work in concentration ratios of $[NO_2]/[Cl^-]$ greater than 0.7 to 1.0, depending on different material and environmental factors. If insufficient quantities are reached, the anodic nature of the inhibitor, as well as any other anodic inhibitor, may aggravate the corrosion, leading to pitting *(52)*.

Additionally, since the inhibitor is soluble, there is a possibility of it leaching from the concrete and severely reducing the corrosion inhibition effectiveness. In addition, its use results in concern related to its toxicity and possible environmental damage as nitrite is known to cause health problems *(53,54)*.

In the interest of health and environmental safety, green organic corrosion inhibitors are a great option for inhibiting corrosion in reinforced concrete. The difference between these options of non-green and green organic corrosion inhibitors is that the latter considers the reduction of harmful additives that can be toxic to users and the environment both during the synthesis and the use of the product *(55)*. Common green inhibitors are synthesized from plant extracts and are biodegradable *(56,57)*.

A green synthesized organic compound, 1-Benzyl-4 Phenyl-1H-1,2,3-Triazole (BPT) was proposed to be used as a corrosion inhibitor in reinforced concrete. Fernandes, M.C. et al *(55)* reported the use of BPT as a successful corrosion inhibitor of mild A36 steel in an acidic environment (1 M HCl). The synthesis of the BPT involved in this project removes long synthetic procedures and the production of toxic additives that allows it to be considered green. Additionally, these 1,2,3-Triazole compounds have been noted to be found as biologically active compounds, commonly used in the medicinal industry. As BPT is an organic compound, its suspected method to inhibit corrosion is by chemisorption onto the surface of the steel and then promote growth and maintenance of the protective oxide films. Furthermore, the Tafel polarization curves produced from the work in mild steel classified the inhibitor as a mixed inhibitor, affecting both the anodic and cathodic reactions.

4. METHODOLOGY

4.1. Geopolymer Synthesis

The GPs used in this research were synthesized by researchers using sodium or potassium hydroxide (Noah Technologies, TX), amorphous fumed silicon (IV) oxide (Alfa Aesar, MA) with 350- 410 m^2/g specific surface area, MetaMax® (BASF Catalysts LLC, NJ) metakaolin, and deionized water. Metakaolin is a purer aluminosilicate source than the more commonly used fly ash with higher impurities and was therefore used as a precursor for GP synthesis in this research.

The potassium hydroxide was dissolved in deionized water to create a highly alkaline solution to process the alkali metal cations. The amorphous fumed silicon oxide was then added to adjust the SiO_2/Al_2O_3 ratio of the final product as desired, to create the activating solution for the synthesis of geopolymer. The activating solution was then mixed with metakaolin, which is a high-purity activating aluminosilicate source in a high-sheared mixer for 6 minutes at 400 revolutions per minute (RPM) to create a homogenized mixture, known as GP. The general procedure for geopolymer synthesis is shown in Figure 1.

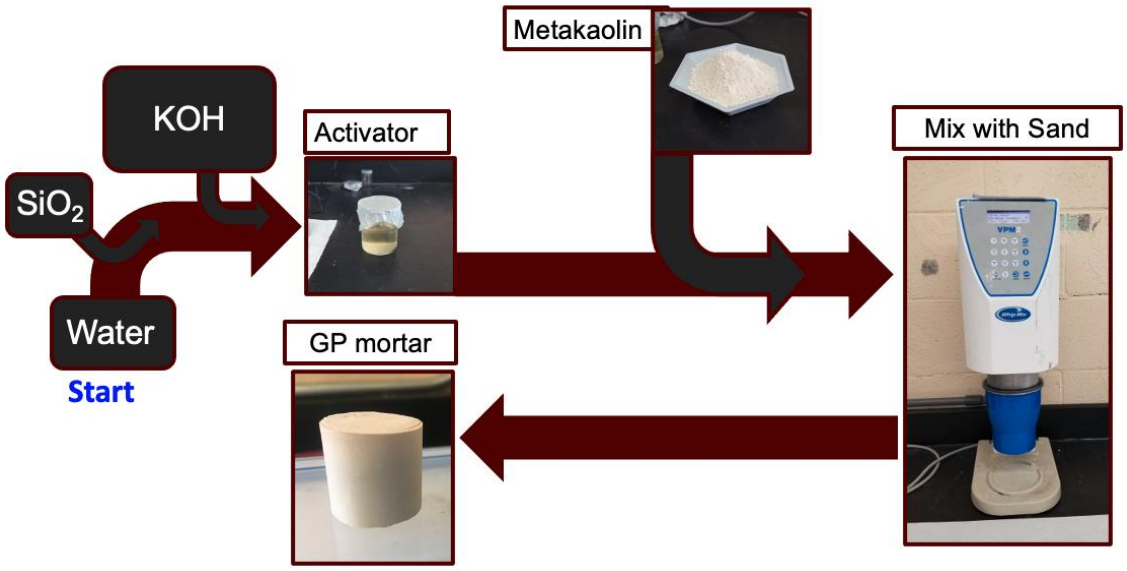

Figure 1. Procedures for geopolymer synthesis.

4.2. Selection of Geopolymer Compositions

Since GPC has 4 chemical parameters, the number of possible compositions is endless and was narrowed down to a few compositions, while still having enough variation to efficiently test the effect for each of the parameters. Based on the work done within Tran-SET project #19CLSU04, several preliminary compositions were chosen because of their good compressive strengths, then the compositions were adjusted so that there is enough number of tests done on each of the 4 parameters. The previous study had 2 phases – during the first phase, 10 compositions were cured for 14 days, then during the second phase, the compositions were narrowed down to 4 based on the results from the first phase for further testing after curing for 28 days. According to the results obtained from the previous #19CLSU04 study, the promising GP conditions were selected as

shown in Table 1. Note that all GPC samples with different compositions are labeled as KXYZ, where the XYZ numbers denote SiO_2/Al_2O_3 ratio, water to solid ratio used to prepare GPC, and K/Al ratio respectively. For example, GPC sample K421 is sample prepared with K-activator, and SiO_2/Al_2O_3=4, water/solid ratio=2, and K/Al=1. To compare the anti-corrosion performance with the OPC concrete samples, the water/cement ratio (or water/binder ratio in the case of GP samples) were calculated for each GP composition.

Table 1. List of GP compositions.

Test Set	K-GP	Water/Binder Ratio
Set 1	K 33(1.2)	0.45
Set 1	K 3(4.3)(1.2)	0.65

4.3. BPT Inhibitor Evaluation

4.3.1. Selection of Optimal BPT Concentration

To select the optimal BPT concentration to be used in mortar specimens, the BPT inhibitor was evaluated in a synthetic pore solution (SPS). The electrochemical experiments followed procedures based in ASTM G59 and ASTM G61. The SPS was prepared with 8.33 g/L NaOH + 23.3 g/L KOH + 2.0 g/L $Ca(OH)_2$ (pH = ~13.51), and deionized water from a Milli-Q® Water Purification System (resistivity: 18.2-18.7 MΩ.cm) and analytical pure grade reagents. The BPT is not very soluble in water, therefore N-methyl-2-pyrrolidone (NMP) was used as a co-dissolver to allow the BPT to dissolve in the SPS. A mother solution with a BPT concentration of approximately 2.35mg/mL in NMP was prepared. Aliquots of this mother solution were used to prepare the test solutions.

The electrochemical tests were performed using a Gamry Reference 600+ Potentiostat. The test cell was a three-electrode setup composed of a platinum mesh as counter electrode (CE), a Saturated Calomel Electrode (SCE) for solutions with chloride or a Mercury Mercurous Sulfate Electrode (MSE) for solutions without chloride as reference electrodes (RE), and a #3 carbon steel reinforcing bar (C 0.41%, Mn 0.57%, P 0.013%, S 0.051%, Si 0.16%, Cu 0.35%, Cr 0.19%, Ni 0.22%, Mo 0.092%, V 0.003%, Cb 0.000%, Sn, 0.012%, Al 0.000%, per the mill report) as the working electrode (WE).

A cylindrical WE with a length of 10cm was used. Both ends were covered with a coating leaving an exposed area of 4.2cm^2 (Figure 2). Different masking materials were tested (lacquer, paint, epoxy), trying to exclude crevice corrosion on the rebar. In addition, a 1018 carbon steel sample, ½" in length with a 3/8" diameter, provided in a Gamry EuroCell Kit, was also used as WE in 2 of these experiments. The WEs were prepared by polishing with a series of 120-600 grit SiC paper and then submerged in acetone for 5 minutes prior to being introduced in the SPS. Three different electrolytes, shown below, were used in the experiments. The experiments were performed in 550 mL of solution.

- SPS.
- SPS + 0.1 M Cl (5.844g/L NaCl).
- SPS + 0.6 M Cl (35.064g/L NaCl).

The WE was allowed to be submerged in the electrolyte for 24 hours, prior to conducting electrochemical measurements, to allow for passivation and/or activation. The Open Circuit Potential (OCP) was measured prior to the tests to check if the system was in steady-state conditions. The electrochemical measurements performed on the Gamry Potentiostat followed a sequence of OCP, Polarization Resistance (PR), OCP, Electrochemical Impedance Spectroscopy (EIS), OCP, Anodic Cyclical Polarization (CYP), and OCP. The PR was measured from -30mV to +30mV from OCP, with a scan rate of 0.167mV/s, according to ASTM G59. The EIS was measured from 10^5 Hz to 0.001 Hz. The CYP ran at a scan rate of 0.167mV/s, beginning at 30mV more negative than the OCP and with a limiting current density of 1 x 10^{-3} A/cm^2.

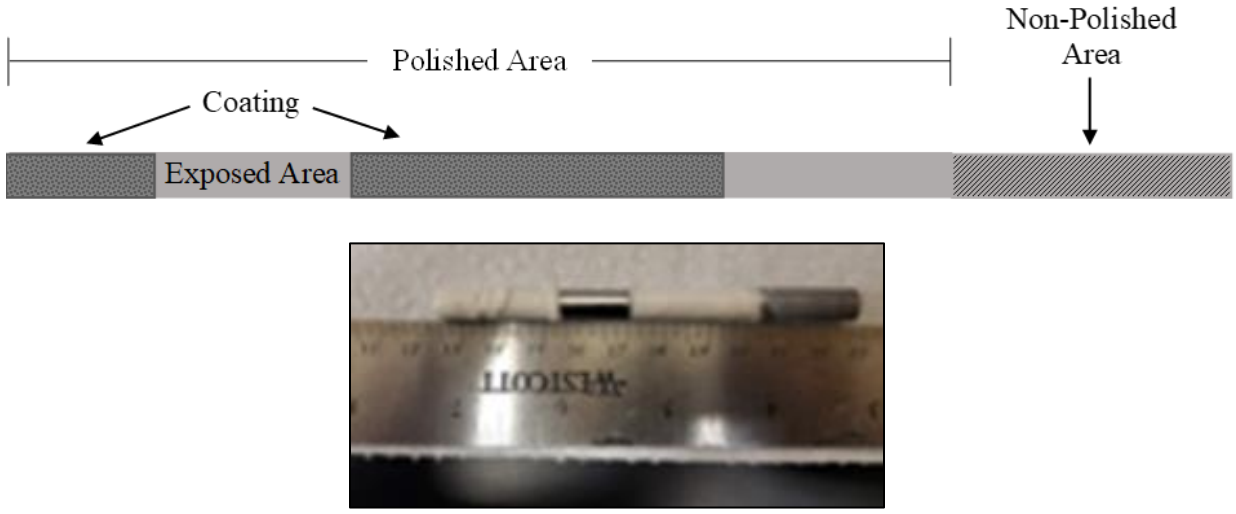

Figure 2. Specimen schematic

Further immersion tests in SPS followed a modified version of the ASTM G180 (74). The electrolytes used in this procedure were based on SPS instead of a cement slurry. In these experiments, the test cell was de-aerated and continuously purged with CO_2-free air throughout the experiment. The #3 carbon steel reinforcing bar used for the WE was cut into 2 cm long specimen and the cross-sectional surface was exposed. These specimens were encased in Ultrabond 2 epoxy coating after tapping a copper wire attached to one face to allow a robust electrical connection to the Potentiostat, with the opposite specimen face polished, following the same procedure mentioned before and leaving an exposed area of 0.498±0.009 cm^2. The conditions displayed in Table 2 were tested with and without chloride (2 M NaCl).

Table 2. Immersion test conditions

Condition	NaOH (g/L)	KOH (g/L)	$Ca(OH)_2$ (g/L)	BPT (mM)	NMP (mL/L)	pH (No Cl)	pH (w/ Cl)
SPS1	8.33	23.3	2	-	-	13.6	13.3
SPS2	8.33	23.3	2	-	100.12	13.5	13.3
SPS3	8.33	23.3	2	-	400.48	14.2	13.6
SPS4	8.33	23.3	2	1	100.12	13.7	13.3
SPS5	8.33	23.3	2	2	200.24	13.7	13.3
SPS6	8.33	23.3	2	3	300.36	13.8	13.4
SPS7	8.33	23.3	2	4	400.48	14.1	13.6

Experiments started by pouring 500 mL of the electrolyte being used, into the test cell. The pH of the solution was measured and then the test cell purged with CO_2-free air for 5 minutes at 300 cc/min, per the ASTM G180 standard, prior to the introduction of the WE. The WE was polished again with 600 grit and ultrasonically cleaned with hexane for 2 minutes prior to being immersed in the electrolyte. The WE was then immersed in the electrolyte for 24 hours while purging the cell . After 24 h, chlorides were added to the cell using analytically pure NaCl and stirred for 4 h using a magnetic stirrer, while continuing to purge the cell. After stirring, the test cell continued to purge for 20 h, prior to the beginning of the electrochemical measurements. If the experiment were to not use chlorides, after the immersion of the WE, the test cell purged for 48 hours straight, prior to the beginning of the electrochemical measurements. The Gamry Potentiostat followed the sequence: OCP, PR, OCP, PR, and then OCP. Each OCP following the steady-state identification (first OCP) was measured for 5 minutes, with a sample period of 0.5s to validate the non-destructive electrochemical techniques performed. Once the electrochemical measurements were completed, the WE was removed from the test cell, and the pH of the electrolyte was measured. The WE was then rinsed and cleaned with ethanol.

4.4. Preparation of Reinforced Samples

4.4.1. Mix Design of Geopolymer-based Cement Mortar Samples

According to the selected geopolymer compositions, the geopolymer mixture was prepared. Based on such geopolymer system, to examine the effect of 1-benzyl-4-phenyl-1H-1,2,3-triazole (BPT) as a green corrosion inhibitor equipped with anti-corrosion function, such inhibitor was add-mixed into the concrete matrix before curing. Additionally, to address with enhanced dissolve of BPT into the synthetic pore solution (SPS), N-methyl-2-pyrrolidone (NMP) was also added into the system. The compositions of each concrete system are shown in Table 3. Please notice the amounts shown in the Table 3 would be based on the size of each batch used during the preparation of mortar samples.

Table 3. List of GP compositions examined in this study.

Sample ID	NMP (mL)	BPT (mM)	w/c ratio
K 33(1.2) + BPT	-	4	0.45
K 33(1.2) + BPT + NMP	957.526	4	0.45
K 3(4.3)(1.2) + BPT	-	4	0.65
K 3(4.3)(1.2) + BPT + NMP	957.526	4	0.65

4.4.2. Mix Design of BPT-based Ordinary Portland Cement Samples

Once the optimal concentration of the BPT inhibitor was determined in the SPS immersion tests, mortar specimens were created to perform electrochemical and physic-mechanical tests. Ordinary Portland Cement (OPC) mortar specimens used a 0.65 w/c mix and Geopolymer (GP) mortar specimens contained both a 0.65 w/c and 0.45 w/c mix. The ACI Standard Practice for Selecting Proportions for Normal, Heavyweight, and Mass Concrete *(50)* was used to design the recipe for mortars. The composition of the mortar mixes used for the specimen utilized tap water, OPC type I/II low alkali, and all-purpose sand that meets ASTM C33 *(58)* requirements for preliminary

mortar tests and silica sand that meets ASTM C778 *(59)* for the actual mortar specimens to be used as fine aggregate (Table 4).

Table 4. Composition of the mortar for 1 m^3

Substances	Mass (kg)
Water	222.21
Cement	341.66
Sand	796.95

Since the electrochemical tests in SPS solutions indicated that the optimal concentration of the inhibitor was between 2-3 mM BPT, the mortars were prepared with concentrations of 2, 2.5 and 3 mM BPT. These mortars were used to conduct OCP and PR, following ASTM C876 *(60)* and ASTM G59 *(61)*, respectively, after accelerated exposure per modified ISO11474 *(62)*. The dimensions of the electrochemical mortar specimen molds were 20.5 cm x 10.5 cm x 8.5 cm, but were only filled with mortar mix to a 6 cm height, giving a cover of 3 cm on at least one of the faces (the one exposed to 0.6M NaCl). The following conditions were tested once fully cured (28 days):

- Control
- 2mM BPT
- 2.5mM BPT
- 3mM BPT
- 2.5mM BPT + NMP
- 3mM BPT + NMP

The molds used for the mortar specimens were sprayed with vegetable oil and wiped down to gather any excess at least 30 minutes prior to the pouring of the mortar mix, to allow the specimens to be easily removed after dry curing. If the condition utilized both BPT and NMP, a mother solution was created and allowed to magnetically stir for 1 hour prior to adding to the mix. After the sand and cement amounts were weighed out, half the total water volume needed was added to the sand and mixed for 1 min to allow the fine aggregate to become moistened. The cement amount was then added to the mix. For the control condition, the other half of the water volume was added with the cement. For conditions containing BPT only, the inhibitor was added into the cement and mixed, prior to being added to the main mix, with the other half of the water volume added soon after. For conditions with both, BPT and NMP, the amount of the mother solution created was accounted for the total liquid volume, reducing the amount of water in the mix. The BPT and NMP solution was added to the main mix after the cement, with water added afterwards to get to the total liquid volume. The mortar mix was stirred for 5 minutes, allowing the mixture to become homogeneous.

In addition to the geopolymer-based cement concrete, the mix-design of the BPT-based ordinary portland cement concrete samples were also prepared according to Table 5. The targeted water-to-cement ratio (w/c ratio) was 0.65, which potentially allow early-period corrosion initiation of the reinforcing steel, hence the examination of the reinforcing steel with presence or absence of such green-corrosion inhibitor could have been performed in a realistic time horizon. Please notice the

amounts shown in the Table 5 would be based on the size of each batch used during the preparation of mortar samples.

Table 5. List of OPC compositions examined in this study.

Sample ID	Water (kg)	Cement (kg)	Sand (kg)	NMP (mL)	BPT (mM)	w/c ratio
Control	4.52	6.96	16.43	-	-	0.65
2.5 mM BPT	4.52	6.96	16.43	-	2.5	0.65
2 mM BPT	4.15	6.96	16.43		2	0.65
3 mM BPT	4.52	6.96	16.43		3	0.65
2.5 mM BPT + NMP	3.39	6.96	16.43	1132	2.5	0.65
3 mM BPT + NMP	3.17	6.96	16.43	1358	3	0.65

4.4.3. Sample Preparation Procedure and Preliminary Results with BPT-added Mortar

The procedure to make the mortar specimen is as follows:

1. 30 minutes prior to creating the mortar mix, spray the mold with vegetable oil. Wipe down any excess.

2. Weigh amount of sand, cement, and water needed.

3. In a mixing bowl, pour the sand and half of the water amount, then mix together for 1 minute to allow the sand to become saturated with the water.

4. Pour the cement and half the water amount into the mixing bowl, then mix together for 5 minutes or until the mix is homogeneous.

a. If evaluating BPT only, introduce BPT amount with cement amount. Mix into cement prior to introduction.
b. If evaluating BPT + NMP, create solution prior to introduction and introduce with half of water for cement. Account for water added by subtracting regular volume amount presented in table, by the BPT + NMP solution volume.

5. Pour mortar mix, once homogeneous, into the mold. Pack the mortar into the mold, then cover with moist paper to avoid evaporation of liquid in the mix.

6. After 24 hours, remove paper from mold. If specimen is not fully cured yet (case of the mortar with NMP), cover surface with a moist paper for an additional 24 hours. Disassemble mold to remove mortar specimen, then immerse specimen in water until ready for experiments.

To understand the effect that the BPT inhibitor and the co-dissolver NMP have on the physic-mechanical properties of mortar specimens and improve the mortar preparation process prior creation of the main specimens, preliminary tests were conducted. The samples were 2 in. mortar cubes prepared following ASTM C109 *(63)*, to observe flow, setting time, and compressive strength. A concentration of 3mM BPT was chosen for evaluation in the mortar cubes as it showed the most optimal performance in the SPS tests. The BPT was evaluated by itself, with the amount of BPT added with respect to the amount of OPC present in the mix, and with NMP, with the amount of BPT and NMP added in respect to the water amount present in the mix. The amount prepared for the mix was enough to create a batch of 6 mortar cubes, plus 20% to account for any errors in the preparation process. Each batch was hand mixed and prepared prior to the afternoon, or late in the afternoon to avoid high temperatures and reduce the evaporation of the water content. The following conditions were tested:

- Control
- BPT
- BPT + NMP

The mortar mix prepared was used to create 3 cubes, with leftover mix to be used for a slump test. The slump test is defined in ASTM C1437, which describes the process to determine the flow of hydraulic cement mortar *(64)*. The test was performed using a flow mold, shaped like a cone, to contain the mortar mix. This mold was placed on top of a flow table, following ASTM C230 [65], and once the mold was full of mortar mix, the mold was removed, and the table was tapped 25 times, allowing the mortar mix to flow and expand. After tapping the table, the diameter of the resulting shape is measured in 4 different directions and recorded. Due to the absence of a flow table, a modified version of the slump test procedure was used. To perform this modified version, a plastic cone with similar dimensions that the one specified in the standard was used and the test was run on a fixed table to make the 25 taps recommended by the standard, before letting the mortar go out of the cone.

The 3 mortar cubes that were prepared, stayed in the mold for 24 hours, or 48 hours if the cubes did not fully solidified yet, while covered with a damp cloth to prevent the evaporation of the liquids. After the cubes were removed from the molds, they were placed in a container filled with tap water to cure. While ASTM C109 *(63)* recommends compression testing at 28 days, due to the availability of testing materials, these cubes were tested after being immersed for 38 days. To perform the compressive tests on these preliminary cubes, a Gilson MC-250CS load frame with a max capacity of 10000 psi, was used.

The designs of the testing specimens are shown in Figures 3 and 4. For the corrosion testing, the concrete sample contained two #3 reinforcing steels with exposed area of 31.35 cm^2, and the size of the concrete specimen was 20.5 cm length, 10.5 cm width, and 6 cm height. The area for the water entrance was designed as 4 inch (~10 cm) by 2 inch (~5 cm). For the mechanical properties of each mortar composition, 2 inch cube samples were also prepared. Furthermore, to measure the porosity throughout the concrete matrix, the cylindrical shaped specimens were also prepared with their dimension of 10 cm diameter and 3 cm height. For the corrosion testing specimens, the mix was poured into the mortar molds containing 2 #3 carbon steel rebars which have mill specifications listed in Table 6. The rebars were shear cut into 10 in. long specimen. Once cut, copper wires were soldered onto each end of the rebar specimen. The rebars were then sandblasted using glass bead abrasive media with a 120-150 grit, then degreased with acetone. An exposed

section with a 10 cm length was masked using Macropoxy 646. The epoxy was applied to the ends of the rebar, then cured for 3 days at room temperature. Prior to insertion to the electrochemical molds (Figure 3), the exposed area was degreased with acetone.

Once casted, the mortar mixes stayed in their molds for at least 24 h, or 48 h depending on if the sample has not set, while covered with a damp cloth. Once solidified, the specimens were carefully removed from the molds to begin the curing process.

Table 6. Chemical composition of rebars used in electrochemical test mortar specimen

	%												
Element	**C**	**Mn**	**P**	**S**	**Si**	**Cu**	**Cr**	**Ni**	**Mo**	**V**	**Cb**	**Sn**	**Al**
Batch 1	0.41	0.57	0.013	0.051	0.16	0.35	0.19	0.22	0.092	0.003	0.000	0.012	0.000
Batch 2	0.44	0.64	0.009	0.041	0.17	0.33	0.07	0.12	0.039	0.000	0.000	0.012	0.001

4.4.4. Electro-Chemical and Physical-Mechanical Characterization of the Mortar

Following the same mortar preparation in section 4.4.4, the sample conditions were also prepared in molds of different dimension depending on the type of test to be performed as specified below. In terms of the curing procedure, the OPC cubes were placed in a tub and immersed in water, while the GP cubes were wrapped in a moist cloth to cure until ready for testing.

Figure 3. Mortar electrochemical molds.

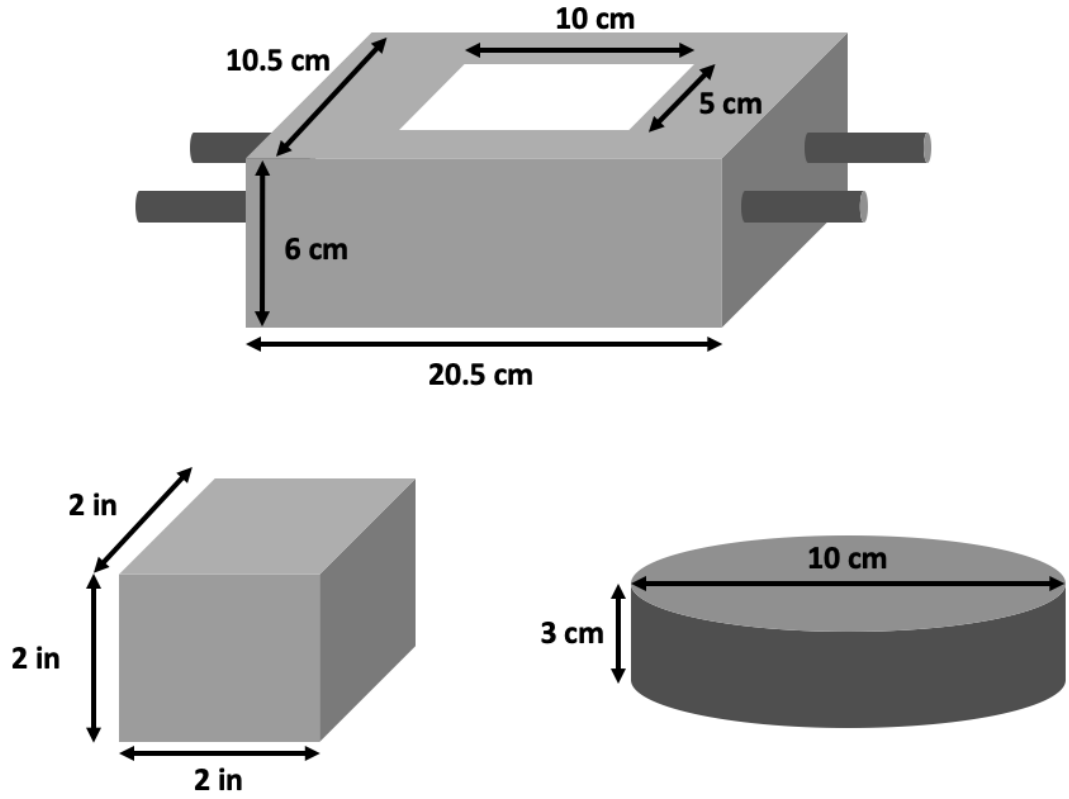

Figure 4. Schematics of samples tested.

4.4.4.1. Compressive testing

These 2 inch mortar cubes followed ASTM C109 standard *(63)* to determine the compressive strength of each of the sample conditions. A Gilson MC-250CS load frame and a MTS 311.31/311.31 load frame were used for the preliminary and actual tests, respectively. The cubes were tested at 31 days.

4.4.4.2. Electrical resistivity

To determine the resistivity of the mortar specimens (10-cm diameter cylinders) to the flow of chloride ions, an electrical resistivity test could was performed *(66)*. These mortar cubes were poured to a height of 3 cm to follow the DURAR manual *(67)* to determine the electrical resistivity of each of the conditions. Once cured to the specified day, a MC Miller 400A soil resistivity meter was utilized to conduct the measurements immediately once the specimens were removed from the curing container.

4.4.4.3. Capillary absorption

The 10-cm diameter mortar cubes were poured to a height of 3 cm to follow the DURAR manual *(67*) to determine the absorption for each of the conditions. These specimens were the same used in the electrical resistivity tests in section 4.2.4b. After the resistivity tests were performed, the specimens were placed in an oven set to 50°C to dry for at least 48 hours and then removed once

weight measurements were consistent between 1-hour readings. The curved surface of the specimen was coated in candle wax to avoid evaporation. The specimens were then weighed and placed on sponges immersed in a tub of water. The water was kept at a level 3 mm above the submerged face of the specimen and the weight of the specimen was recorded at 1/10, 1/6, 1/4, 1/2, 1, 2, 3, 4, 6 h points and then at 24 h points until mass consistency was reached (0.1% difference between consecutive 24h readings). After this test, another resistivity test was performed the curing container.

4.4.4.4. Electrochemical corrosion tests

Modified ISO 11474 Standard (62) was used, as an accelerated test, to evaluate the effect of BPT in mortar, with and without GP. For both the OPC and GP electrochemical test specimen, the exposed rebar on each side of the specimen was wrapped in electrical tape. Then, the specimen was wrapped in a damp paper towel and placed in a plastic bag to cure until ready for environmental exposure per ISO11474 and electrochemical tests (62). The paper towels were kept continuously damp during the curing process and were replaced along with the plastic bags once a week to prevent the growth of microorganisms.

The 0.65 w/c OPC and GP mortar specimens were cured for 28 days, while the 0.45 w/c GP mortar specimens were cured for 7 days prior to exposure and electrochemical testing. Measurements were performed with a Copper/Copper Sulfate (CCS) RE and a Fluke multimeter for OCP measurements to check for stability and a Gamry Potentiostat for LPR tests. These specimens were sprayed, periodically, with a 3.5 wt% NaCl solution once OCP measurements were stable. EIS measurements were also run, using the same procedure indicated in SPS evaluation.

The geopolymer concrete (GPC) samples were prepared according to the results obtained from previous TranSET project No. 19CTAM02, which showed the superior anti-corrosion performance from the composition named K3(2.5)(1.2). Such name represents the cementious geopolymer composition was based on potassium, and the ratio used were SiO_2/Al_2O_3 = 3, water/solid = 2.5, and K/Al, respectively. To properly perform the immersion testing of the concrete specimens, the specimens were mounted with dam to contain the electrolyte as shown in Figure 5, according to ASTM G 109. The mounting of the dam was performed after the curing process. The specification of the dam area was 2” x 2” mounted with epoxy resin. The mounted dam was filled with 200 mL 3.5 wt.% NaCl electrolyte to simulate the sea water condition. More detailed experimental set-up can be found in the project report No. 19CTAM02.

It is important to mention that, although these specimens were prepared according to ASTM G 109, a different electrochemical evaluation was carried out, using the EIS technique, which gives more information about the mechanism than the techniques indicated in that standard. Then, the corrosion performance of the produced GPC samples was characterized by electrochemical impedance spectroscopy (EIS) at room temperature with applied electrolyte. The EIS is a powerful non-destructive technique that allows the user to monitor, characterize, and determine the performance of the RC system and efficiency in different environments. A large number of corrosion results under immersed concrete tests have been analyzed on visual inspection, which is dependent on one’s individual viewpoint and could not be explained quantitatively. To overcome the qualitative weakness of visual inspection EIS is utilized to quantitatively monitor the electrochemical processes of the system while it is under constant immersion condition. A schematic illustration of EIS is shown in Figure 6.

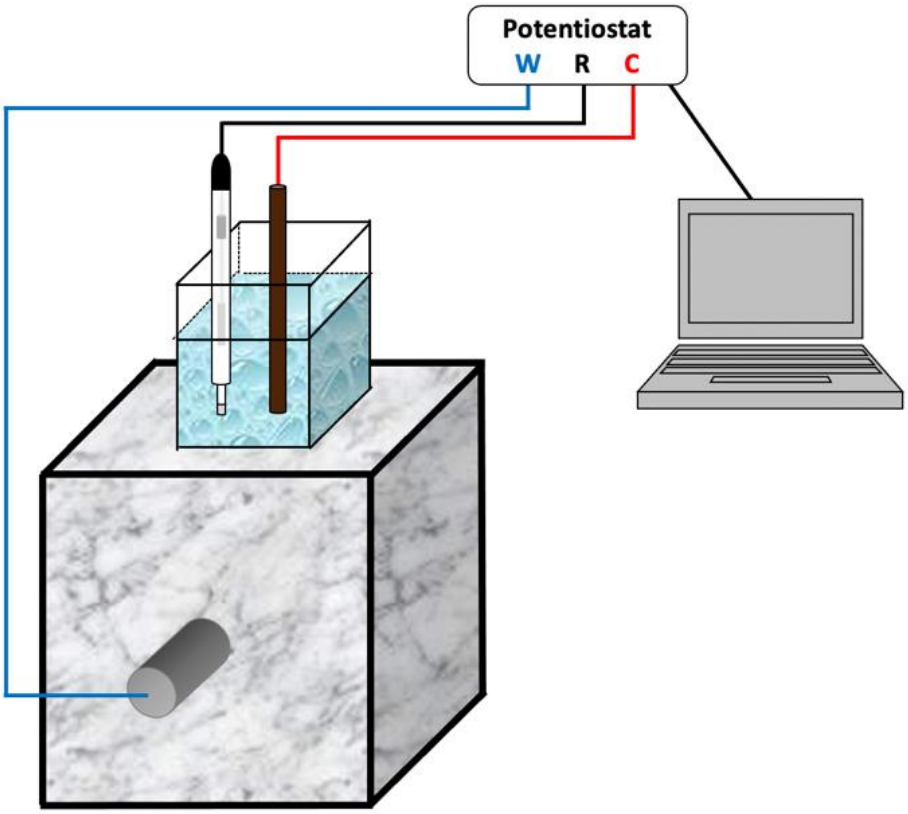

Figure 5. Schematics of the electrochemical testing.

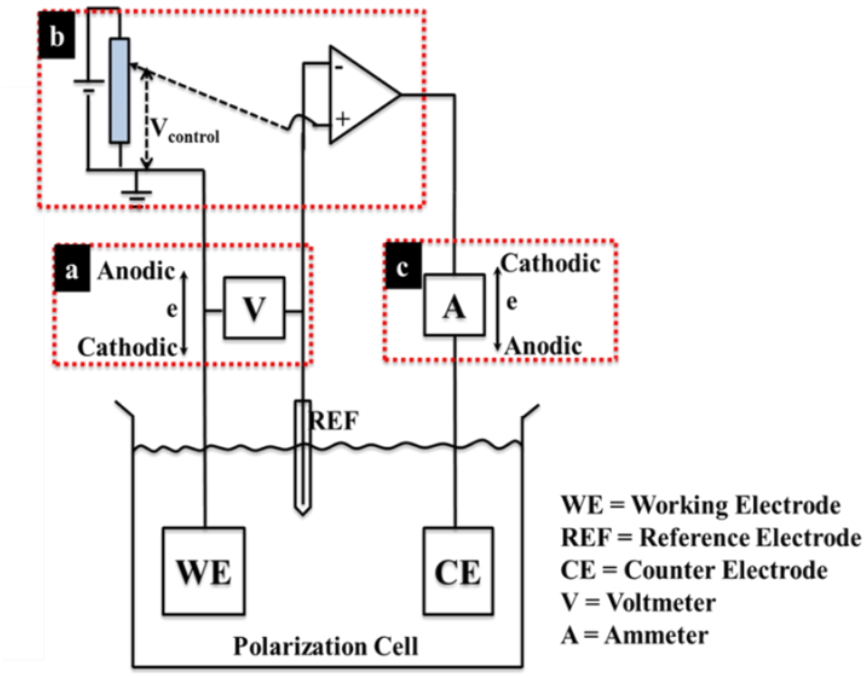

Figure 6. Conventional three-electrode system.

The constant immersion testing was performed using the aforementioned dam filled with 200 mL of 3.5 wt% NaCl electrolyte with an exposed area of 24.55 cm^2 using the Gamry 1000E Potentiostat/Galvanostat. The rebar substrates which were samples of interest, were used as the working electrodes (WE), while graphite rod which was an inert electrode was used for passage of current worked as a counter electrode (CE). A saturated calomel electrode (SCE) was used as a reference electrode (RE) to measure the potential. The test sequence involved 20 minutes of open circuit potential (OCP) followed by EIS at frequencies of 100 kHz to 0.03 Hz with 10 points per decade and an amplitude of 10 mV rms.

4.4.4.5. Fog Chamber Testing

The samples were also tested with ASTM B117 that illustrates the accelerated water uptake through fog-chamber testing. To perform the test, the design of the reinforced concrete specimen was adapted as shown in the previous figure. In addition to such specimen, the specimen was also covered by epoxy coating except the water entrance area, which have allowed to assume that the water with aggressive chloride ion only have penetrated through the entrance without multi-directional chloride uptake. As such assumption was possible, we also could have applied the Fick's first law to describe the diffusional behavior of the chloride ions upon the specimen was exposed to electrolytes that contains aggressive ions, such as chloride ions. Such experimental set-up is illustrated in Figures 7 and 8. The ASTM B117 test was performed at 35 Celsius with 25 psi pressure for 720 hours.

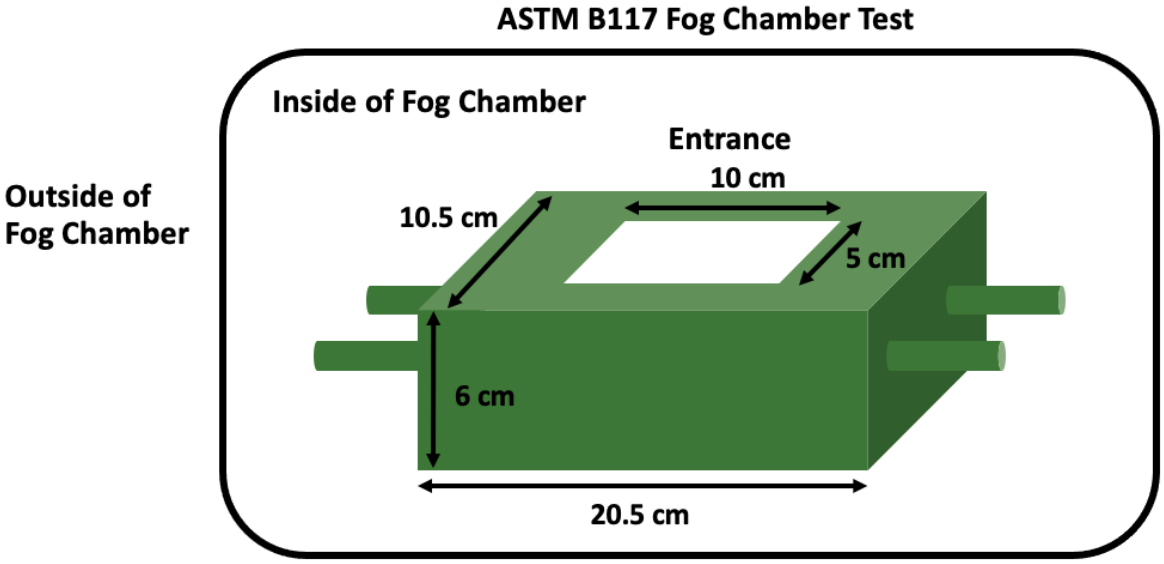

Figure 7. Schematics for fog-chamber testing under ASTM B117.

Figure 8. Fog-chamber testing under ASTM B117.

5. ANALYSIS AND FINDINGS

5.1. Corrosion Behavior of the Geopolymer-based Cement Concrete Samples

5.1.1. Open-Circuit Potential

Figure 9 depicts the open circuit potential (OCP) trends over the testing period for the geopolymer sample with the selected composition. The results from OCP can provide a qualitative indication of the embedded rebar's corrosion activity. The potential difference between the standard reference electrode and the steel rebar as working electrode was used to assess the corrosion of the sample. In this experiment, the criterion suggested previously was applied to understand the regime that the rebar experience. From such figure, it can be observed that the OCP of the K 33(1.2) sample has a constant and repeatable trend around the low to intermediate corrosion risk until the 75 days of immersion in 3.5 wt.% NaCl electrolyte, and in the case of epoxy coated sample a longer period of rebar protection was observed. This is indicative that the sample matrix formed with such binder can effectively delay the water uptake which contains corrosive species, such as chloride ions. By providing such barrier effect, the rebar embedded within the sample could have been well-protected up around two months without proceeding to the severe corrosion regime.

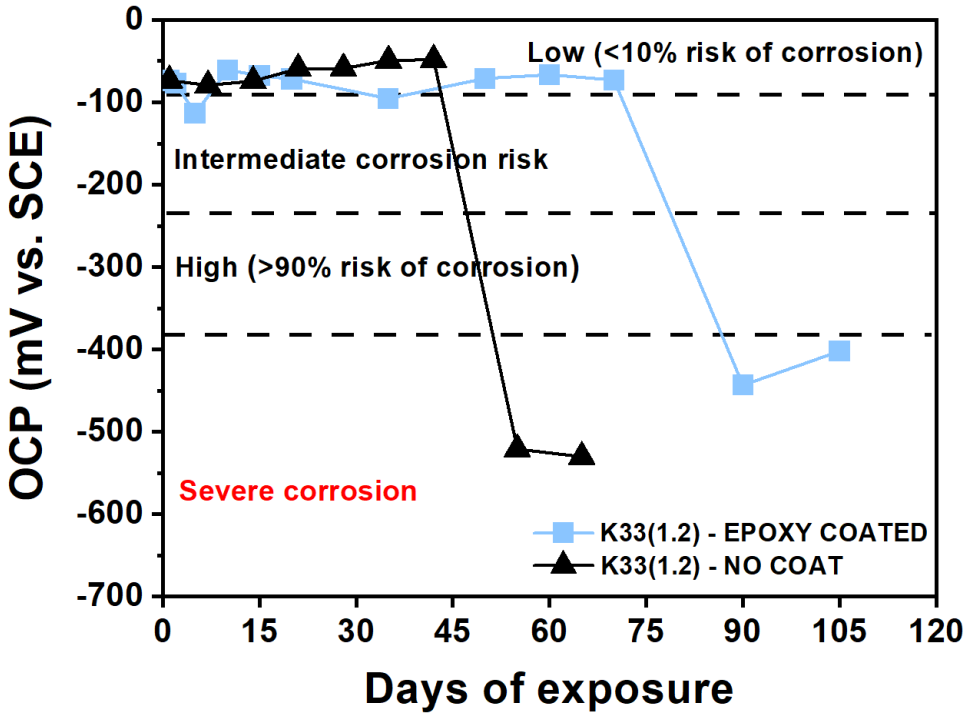

Figure 9. OCP trend of the K 33(1.2) geopolymer samples.

However, we can also observe the earlier breakdown of the reinforcing rebar in case of that there is no epoxy coating around the concrete sample. This can be owing to the evaporation of the electrolyte at the exposed surface of concrete. Specifically, once the electrolyte penetrates throughout the concrete matrix, and reach to any certain concrete surface that is exposed to the environment with air, such electrolyte evaporated and caused enhanced penetration of electrolyte

into the concrete system. As such enhanced penetration of electrolyte also have brought the more of corrosive ions, e.g. chloride ions, into the concrete system, it is reasonable to estimate that the critical chloride ion concentration could have met in an earlier manner, which may have caused the corrosion initiation of reinforcing steel in an earlier manner. Such early degrading trend of the reinforcing steel is well-illustrated in the OCP trend following the ASTM corrosion criteria for reinforced concrete system shown in Figure 10, and due to the introduction of high chloride ion concentration we can observe the earlier entrance of the OCP values into the severe corrosion range in case of the absence of epoxy coating layer on top of the concrete sample.

Copper/copper sulphate	*Silver/silver chloride/ 1.0M KCl*	*Standard hydrogen electrode*	*Calomel*	*Corrosion condition*
>−200 mV	>−100 mV	+120 mV	>−80 mV	Low (10% risk of corrosion)
−200 to −350 mV	−100 to −250 mV	+120 to −30 mV	−80 mV to −230 mV	Intermediate corrosion risk
<−350 mV	<−250 mV	−30 mV	<−230 mV	High (>90% risk of corrosion)
<−500 mV	<−400 mV	−180 mV	<−380 mV	Severe corrosion

Figure 10. ASTM corrosion criteria for reinforced concrete (15).

5.1.2. Electrochemical Impedance Spectroscopy

Figure 11 represents the Nyquist plots of the tested samples obtained by EIS testing for the K 33(1.2) sample. It is observable that the Nyquist plots over the immersion period have similar shape as the typical impedance plots for the concrete samples. Additionally, such plots shown are in a good agreement with the previously shown OCP trend. Specifically, there is no noticeable change with the tail part of the impedance plot, which potentially indicative that the there was no distinctive degradation of the embedded rebar part. Such intact trend was lasted until day 70. After that point, the epoxy-coated K 33(1.2) sample also revealed gradual degradation of its reinforcing steel, indicative that the electrolyte finally uptaked throughout the concrete matrix then reached to the depth of reinforcing steel. Thus, the OCP value which was still maintained at a relatively positive side finally tended to decrease towards more negative sides then entering to the severe corrosion regime.

Meanwhile, it is also observable that the Nyquist plots get shifted over the prolonged immersion period. This is more dominant especially in the early immersion period, and this would be attributed to the slight segregation of the geopolymer towards the surface which is occurred with the unavoidable sinking of the aggregates, Nevertheless, it is also observable that such rapid electrolyte uptake has been relieved as the uptaking electrolyte reaches to the zone with the aggregate, which follows the designed aggregate/binder ratio. Meanwhile there is still a gradual decrease of the impedance values, especially in the real impedance value, and this suggests that the samples' matrix has been gradually penetrated by the electrolyte with the corrosive species, such as chloride ion and oxygen. However, as the tail part of such plot did not show the decreasing regime until around day 90, which allows estimating that such electrolyte penetrating path may have not reached to the depth that rebar is embedded.

However, when the immersion test was prolonged over 70 days, it was observable that the tail part of the Nyquist plot also tended to be decreased. Such trend is indicative of the electrochemical reactions at the interface between electrolyte and the reinforcing steel, which have caused continuous loss of the corrosion resistance of the steel that also includes the dissolution of metal. Due to the high chloride concentration, it is estimated that the native passive layer of the reinforcing steel may not have provided noticeable barrier protection. In case of the sample without the epoxy coating, the Nyquist plot trend also shows an earlier degradation of metal, which is in a good agreement with the previous OCP trend. Specifically, it is observable that the tail part of the Nyquist plot dramatically decreased at around day 50, and a similar trend is observable until day 65, and both are representing there was an active corrosion regime without any noticeable protection mechanism.

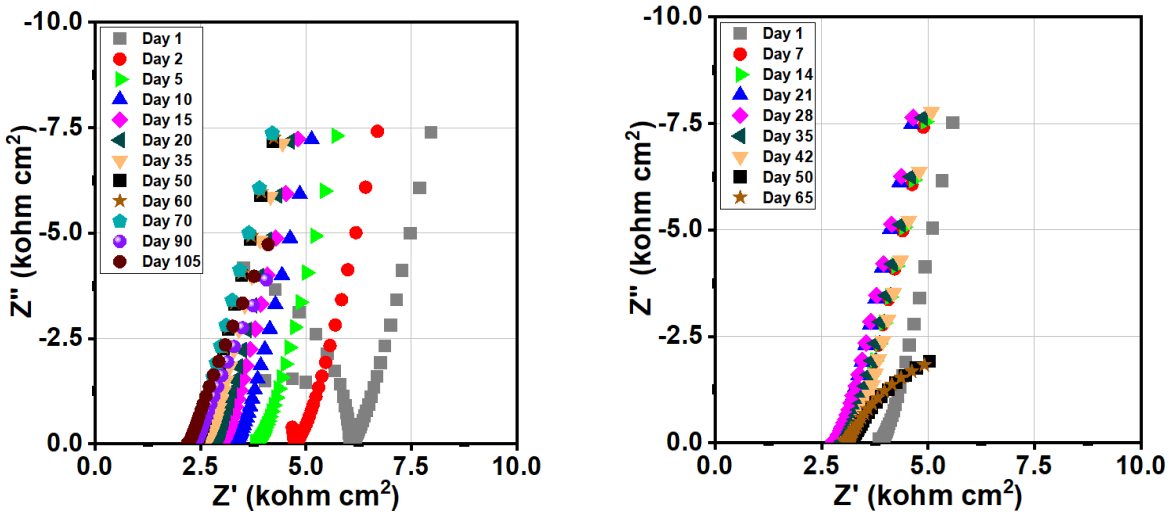

Figure 11. Nyquist plot of trend of the K 33(1.2) geopolymer samples (left-with epoxy coating, right-without epoxy coating).

5.1.3. Deterministic Modeling

Following the electrochemical results, we were able to propose a mechanism base on the dynamics of the interface. The interfacial reactions of the electrolyte up-taking the geopolymer matrix are characterized by EIS. Due to the number of experiments and parameters involved the variability is not considered for this effort. The probabilistic approach is not performed due to the nature of the mechanism. Deterministic approach was implemented based on the elements of the electrochemical system (aqueous electrolyte, solid electrolyte-geopolymer- and rebar) could be studied by deterministic modeling. The theoretical modeling with RC elements and electrolyte characteristics, as well as their validation with electrochemical and concrete testing, allows quantitative approach in regards of the concrete degradation. A simple model based on rebar/concrete interface analysis and real-time monitoring characterization in corrosive environment helped to develop a deterministic approach, as illustrated in this section. Considering the previous EIS results that revealed the general Nyquist plot shape which is also illustrated in Figure 12, we could have addressed the contribution of each element within the concrete system

by identifying them as concrete bulk, bulk-electrode hybrid, and electrode interface, and also able to quantifying the effect of each operator in such electrochemical system. Due to the relatively fast material degradation of the GPC compared to that of conventional OPC, the merit that comes from the probabilistic modeling is not considerable as much as the one from the deterministic modeling, therefore only the deterministic modeling has been studied to better understand the concrete degradation in a quantitative manner.

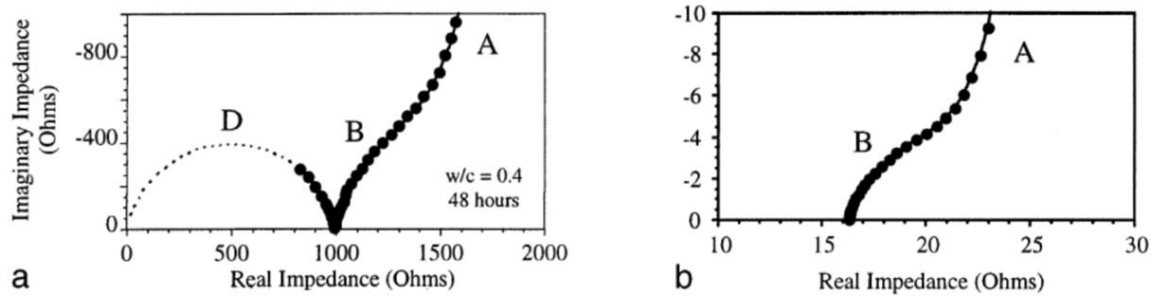

Figure 12. Nyquist plot of carbon steel electrodes in (a) ordinary portland cement and (b) synthetic pore solution [68].

Based on this conceptual understanding of the electrochemical system composition, an electrical equivalent circuit (EEC) model is suggested as shown in Figure 13 to provide effective parameters quantitatively in the corroding system. The impedance spectra that included the concrete bulk, bulk-electrode hybrid, and electrode interface are allocated for each segment of the equivalent circuit component, respectively.

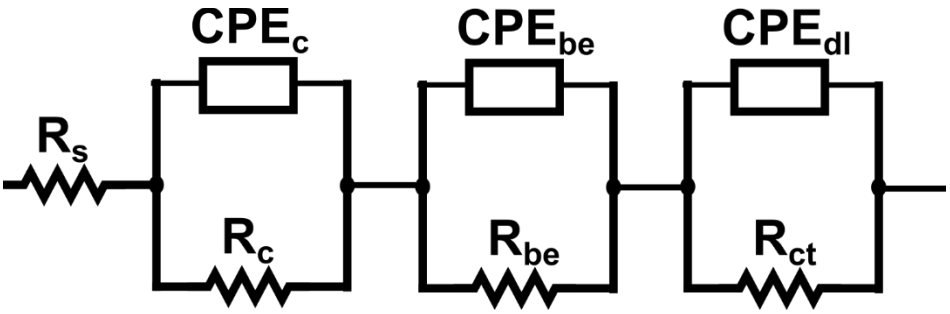

Figure 13. Electrical equivalent circuit for the concrete system.

The ECs included elements, namely, the solution resistance (R_s), concrete bulk resistance (R_c), bulk-electrode resistance (R_{be}), charge-transfer resistance (R_{ct}), capacitance in terms of the constant phase element (CPE), concrete bulk pore capacitance (Q_c), bulk-electrode capacitance (Q_{be}), and double-layer capacitance (Q_{dl}). The CPE concept was introduced to represent the depressed impedance semicircles, which is known to be occurred from the various physical properties of the concrete resulting in the time constants distributions [69,70]. The CPE capacitance can be described as below

$$C = Y_0(\omega''_{max})^{n-1}$$

where Y_0 and $0 < n \leq 1$ are the model parameters, and ω''_{max} is the angular frequency at the maximum imaginary impedance Z''.

The quantified impedance parameters obtained from the aforementioned ECs are summarized in Table 7. During the immersion period, the K 33(1.2)-epoxy coated sample revealed the gradual decrease of both concrete bulk resistance (R_c) and bulk-electrode resistance (R_{be}), and this can be due to the water uptake throughout the concrete matrix including the partially segregated geopolymer cement layer. It is also noticeable that the charge-transfer resistance (R_{ct}) does not change until the immersion day of 70, which is indicative that the reinforcing itself was successfully protected from corrosion reactions from the corrosive electrolyte by the presence of geopolymer concrete matrix. Nevertheless, it is also observable the decrease of R_{ct} after day 70, and such also have caused the increase of double-layer capacitance (Q_{dl}). These trends are illustrative of the degradation of the reinforced steel in terms of electrochemically activated regime. This could have caused by the penetration of the corrosive electrolyte throughout the concrete matrix that finally reached to the rebar interface, then started the electrochemical reactions at the electrolyte/metal interface. Due to the extensive charge transfer reactions, the interface continuously loses semi-capacitive behavior while revealing the charged double layer features.

In case of the K 33(1.2)-no epoxy coated sample also represented a similar trend. However, somewhat accelerated degradation of the concrete system was observable represented by the fitting results including the decreased R_c and R_{be} in the relatively earlier period. Such could have occurred by the enhanced water uptake as the electrolytes reached to the concrete surface level could have been evaporated by the surrounding environment which also may have triggered the faster accumulation of chloride ions within the concrete system. Therefore, the decrease of the R_{ct} along with the increase of Q_{dl} was observed from earlier period, such as day 50 of immersion. It is also estimated the higher chloride ion due to the accumulation during immersion test that has occurred within the concrete matrix of the K 33(1.2)-no epoxy coated sample may also have caused a relatively faster degradation of the reinforcing steel represented by the value of polarization resistance, $R_p = R_c + R_{be} + R_{ct}$, which was lower than the case of K 33(1.2)-epoxy coated sample.

Table 7. Impedance parameters for the GPC samples immersed in 3.5 wt.% NaCl electrolyte.

Time (day)	R_c ($\Omega\ cm^2$)	Q_c ($F\ cm^{-2}\ s^{n-1}$)	n_c	R_{be} ($\Omega\ cm^2$)	Q_{be} ($F\ cm^{-2}\ s^{n-1}$)	n_{be}	R_{ct} ($\Omega\ cm^2$)	Q_{dl} ($F\ cm^{-2}\ s^{n-1}$)	n_{dl}	R_p ($\Omega\ cm^2$)
K 33(1.2)-Epoxy Coated										
1	6.1×10^3	6.4×10^{-10}	0.99	6.0×10^3	9.9×10^{-4}	0.59	1.2×10^5	8.1×10^{-4}	1	1.3×10^5
2	4.7×10^3	8.3×10^{-11}	0.92	4.6×10^3	9.9×10^{-4}	0.53	1.2×10^5	7.4×10^{-4}	0.98	1.3×10^5
5	3.8×10^3	1.7×10^{-9}	0.57	4.5×10^3	9.9×10^{-4}	0.56	1.2×10^5	7.7×10^{-4}	0.99	1.3×10^5
10	3.3×10^3	2.0×10^{-10}	0.81	4.2×10^3	1.1×10^{-3}	0.54	1.2×10^5	7.5×10^{-4}	0.98	1.3×10^5
15	3.0×10^3	2.7×10^{-10}	0.78	3.9×10^3	1.1×10^{-3}	0.54	1.2×10^5	7.2×10^{-4}	0.97	1.3×10^5
20	2.8×10^3	6.2×10^{-10}	0.71	3.7×10^3	1.3×10^{-3}	0.56	1.2×10^5	7.2×10^{-4}	0.96	1.3×10^5
35	2.6×10^3	1.9×10^{-10}	0.84	3.6×10^3	1.3×10^{-3}	0.57	1.2×10^5	7.2×10^{-4}	0.96	1.3×10^5
50	2.4×10^3	3.0×10^{-10}	0.79	3.5×10^3	1.3×10^{-3}	0.58	1.2×10^5	7.3×10^{-4}	0.96	1.3×10^5
60	2.4×10^3	5.0×10^{-10}	0.71	3.5×10^3	1.2×10^{-3}	0.59	1.2×10^5	7.2×10^{-4}	0.96	1.3×10^5
70	2.3×10^3	8.0×10^{-10}	0.69	2.3×10^3	1.2×10^{-3}	0.59	1.2×10^5	7.1×10^{-4}	0.96	1.2×10^5
90	2.4×10^3	7.9×10^{-10}	0.70	2.4×10^3	1.7×10^{-3}	0.62	2.1×10^4	1.4×10^{-3}	0.95	2.6×10^4
105	2.2×10^3	7.0×10^{-10}	0.70	2.2×10^3	1.5×10^{-3}	0.62	3.0×10^4	1.1×10^{-3}	0.94	3.4×10^4
Time (day)	R_c ($\Omega\ cm^2$)	Q_c ($F\ cm^{-2}\ s^{n-1}$)	n_c	R_{be} ($\Omega\ cm^2$)	Q_{be} ($F\ cm^{-2}\ s^{n-1}$)	n_{be}	R_{ct} ($\Omega\ cm^2$)	Q_{dl} ($F\ cm^{-2}\ s^{n-1}$)	n_{dl}	R_p ($\Omega\ cm^2$)

K 33(1.2)-No Epoxy Coated										
1	3.9×10^{3}	2.1×10^{-10}	0.77	4.4×10^{3}	1.1×10^{-3}	0.57	1.2×10^{5}	7.5×10^{-4}	1	1.3×10^{5}
7	3.0×10^{3}	7.0×10^{-10}	0.70	3.5×10^{3}	9.2×10^{-4}	0.57	1.2×10^{5}	7.6×10^{-4}	1	1.3×10^{5}
14	3.0×10^{3}	9.9×10^{-10}	0.66	3.5×10^{3}	9.2×10^{-4}	0.58	1.2×10^{5}	7.4×10^{-4}	1	1.3×10^{5}
21	2.8×10^{3}	1.1×10^{-9}	0.66	3.4×10^{3}	9.7×10^{-4}	0.58	1.2×10^{5}	7.5×10^{-4}	1	1.3×10^{5}
28	2.8×10^{3}	7.4×10^{-10}	0.68	3.4×10^{3}	1.0×10^{-3}	0.57	1.2×10^{5}	7.2×10^{-4}	0.99	1.3×10^{5}
35	3.0×10^{3}	2.3×10^{-9}	0.59	3.7×10^{3}	9.9×10^{-4}	0.58	1.2×10^{5}	7.4×10^{-4}	1	1.3×10^{5}
42	3.2×10^{3}	2.7×10^{-9}	0.57	3.7×10^{3}	1.0×10^{-3}	0.55	1.2×10^{5}	7.0×10^{-4}	0.99	1.3×10^{5}
50	3.2×10^{3}	2.9×10^{-9}	0.59	2.6×10^{3}	2.5×10^{-3}	0.56	4.3×10^{3}	1.6×10^{-3}	0.83	1.0×10^{4}
65	3.1×10^{3}	2.1×10^{-9}	0.61	2.2×10^{3}	2.4×10^{-3}	0.53	4.2×10^{3}	1.6×10^{-3}	0.83	9.5×10^{3}

5.2. Evaluating BPT Effect

5.2.1. Electrochemical Evaluation in SPS

The polarization resistance, Rp, values measured from the different conditions are presented in Figure 14. The Rp values were taken from the resulting PR plot as the slope at the value at which i = 0 A/cm^2, following ASTM G102 *(71).* The corrosion rate of the metal can be taken from the Rp using the Stern-Geary equation *(61).* This equation [1] calculates the corrosion current density, i_{corr}, as shown:

$$i_{corr} = \frac{\beta_a \times \beta_c}{2.303 \times R_p(\beta_a + \beta_c)} = \frac{B}{R_p} \quad [1]$$

The parameters of βa and βc represent the anodic and cathodic Tafel slopes, respectively. These are both taken equal to 0.12 V, resulting in a Stern-Geary coefficient, B = 0.026 V *(67).* It is well known that for active conditions, B has a value in the order of 26mV and for passive conditions, a value in the order of 52mV, which means 26mV is a good value to use for all the conditions. It is also the value used in the commercial equipment to evaluate corrosion rate of reinforcement. The units of Rp are ohm-cm^2 and following the necessary conversions to present i_{corr} in units of μA/cm^2, the corrosion rate (CR) of the carbon steel rebar was determined using the following equation [2]:

$$CR = 3.27 \times 10^{-3} \frac{(i_{corr} \times EW)}{\rho} \quad [2]$$

The coefficients EW and ρ represent the equivalent weight and density of the corroding species, which in the case of carbon steel was taken as EW = 27.92 g and ρ = 7.87 g/cm^3 *(71).* The resulting CR is presented in mm/year in Figure 15.

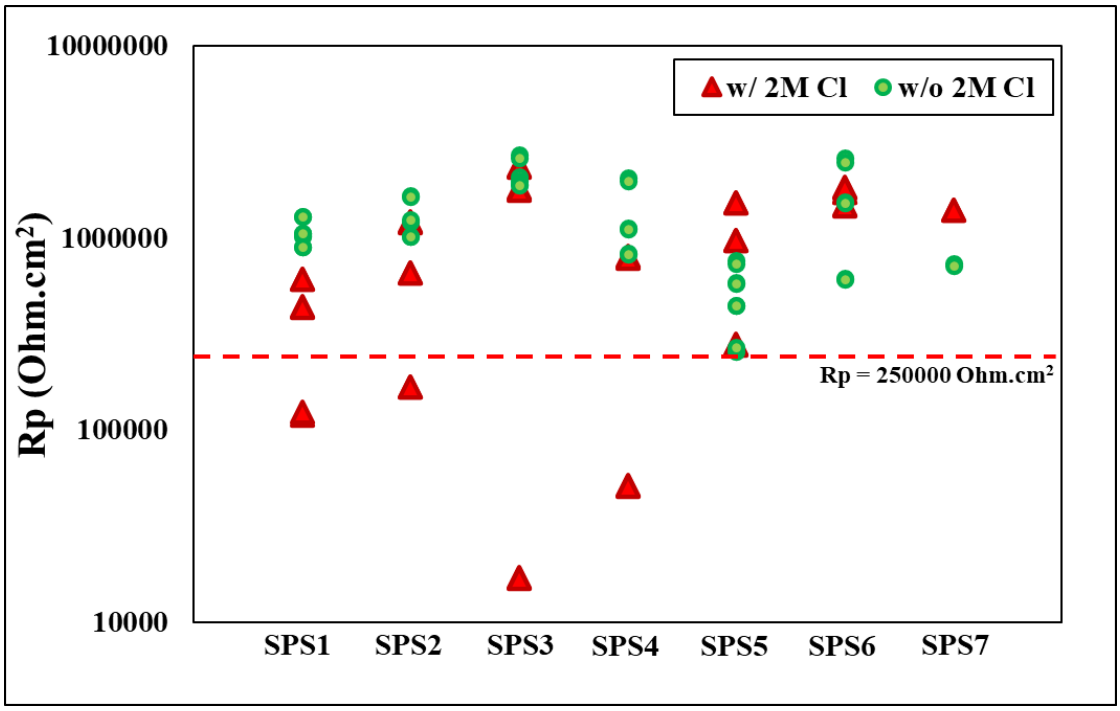

Figure 14. Polarization resistance values from SPS immersion tests seen in Table 2 (SPS1 = SPS, SPS2 = SPS + 100 mL NMP, SPS3 = SPS + 400 mL NMP, SPS4 = SPS + 1 mM BPT + 100 mL NMP, SPS5 = SPS + 2 mM BPT + 200 mL NMP, SPS6 = SPS + 3 mM BPT + 300 mL NMP, SPS7 = SPS + 4 mM BPT + 400 mL NMP)

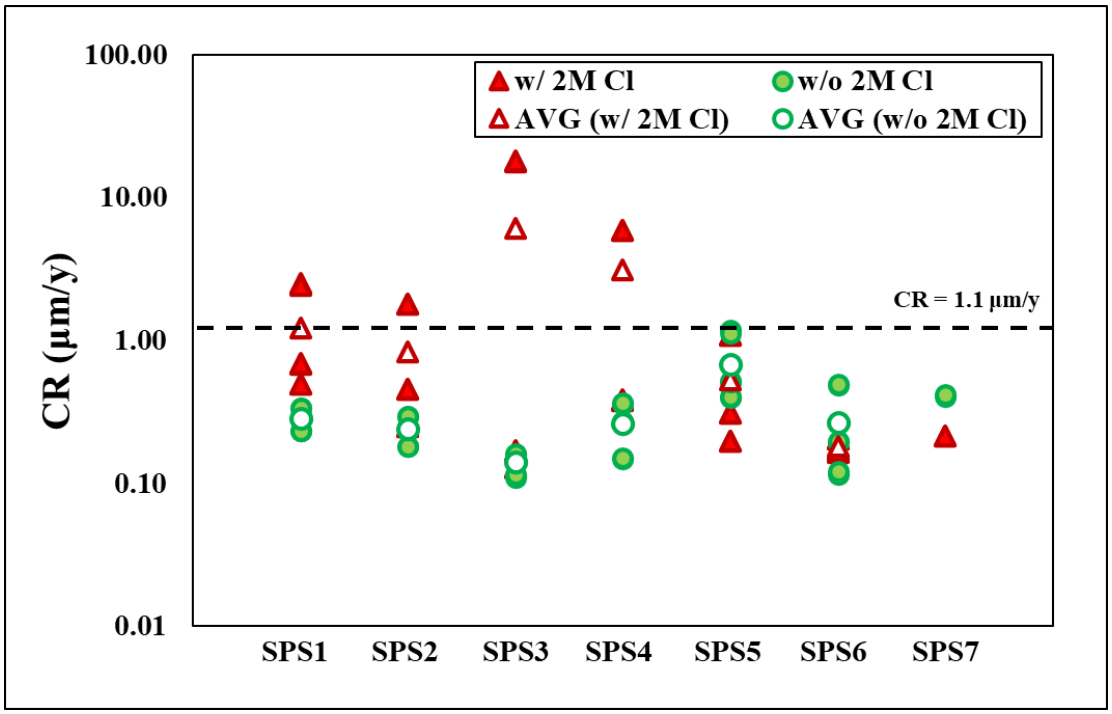

Figure 15. Corrosion rate values from SPS immersion tests seen in Table 2 (SPS1 = SPS, SPS2 = SPS + 100 mL NMP, SPS3 = SPS + 400 mL NMP, SPS4 = SPS + 1 mM BPT + 100 mL NMP, SPS5 = SPS + 2 mM BPT + 200 mL NMP, SPS6 = SPS + 3 mM BPT + 300 mL NMP, SPS7 = SPS + 4 mM BPT + 400 mL NMP

For conditions containing 2mM of BPT, the corrosion rate decreased. The high values for condition SPS3 (higher amount of NMP) can be attributed to the high pH value (pH > 14), where higher values of pH require more chlorides to break the passive film. In Figure 14 there is a dashed red line in which points above show evidence of a passive film formed on the carbon steel rebar surface, protecting it in the SPS solutions (corrosion rate lower than 0.1 µA/cm^2 or1.1 µm/y) *(67)*; which is also shown in Figure 15. At concentrations above 3mM, a decrease in effectiveness is seen, leading to the assumption that the optimal concentration lies somewhere between 2 and 3mM BPT.

The effectiveness of BPT is also confirmed in subsequent EIS tests where the Nyquist plots show greater half-circle diameters as the concentration of the BPT increases, showing better protection of the rebar surface (Figure 16). The effect is continued with the SPS3 condition, again due to the high pH of the solution, creating a stronger passive film on the rebar.

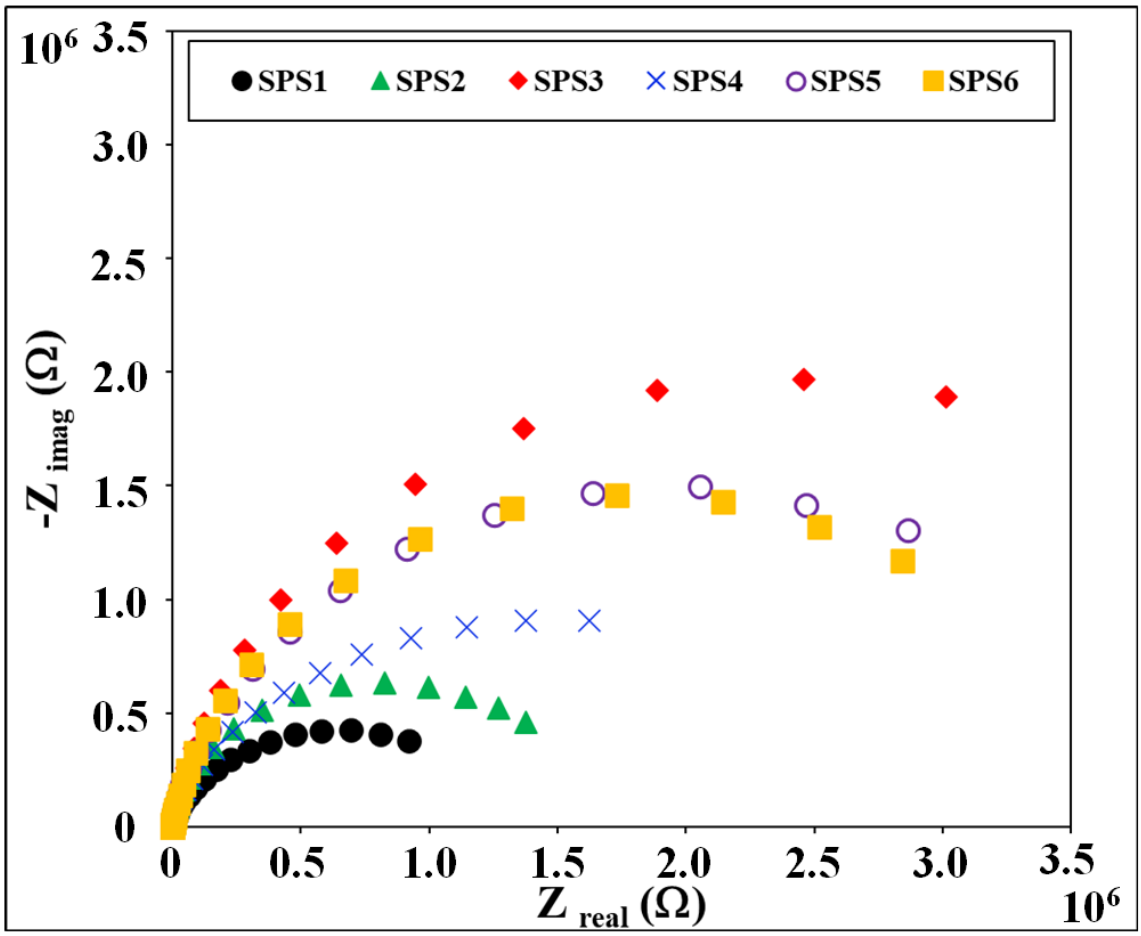

Figure 16. Nyquist plot of SPS with 2 M Cl immersion tests (SPS1 = SPS, SPS2 = SPS + 100 mL NMP, SPS3 = SPS + 400 mL NMP, SPS4 = SPS + 1 mM BPT + 100 mL NMP, SPS5 = SPS + 2 mM BPT + 200 mL NMP, SPS6 = SPS + 3 mM BPT + 300 mL NMP, SPS7 = SPS + 4 mM BPT + 400 mL NMP

Following the LPR and EIS tests, anodic cyclical potentiodynamic polarization measurements were made. As can be seen in Figure 17, the pitting potentials increased with increasing BPT concentrations. The final range of potential was increased to see if the carbon steel rebar specimens could produce a repassivation potential, but no condition was able to repassivate prior to reaching OCP.

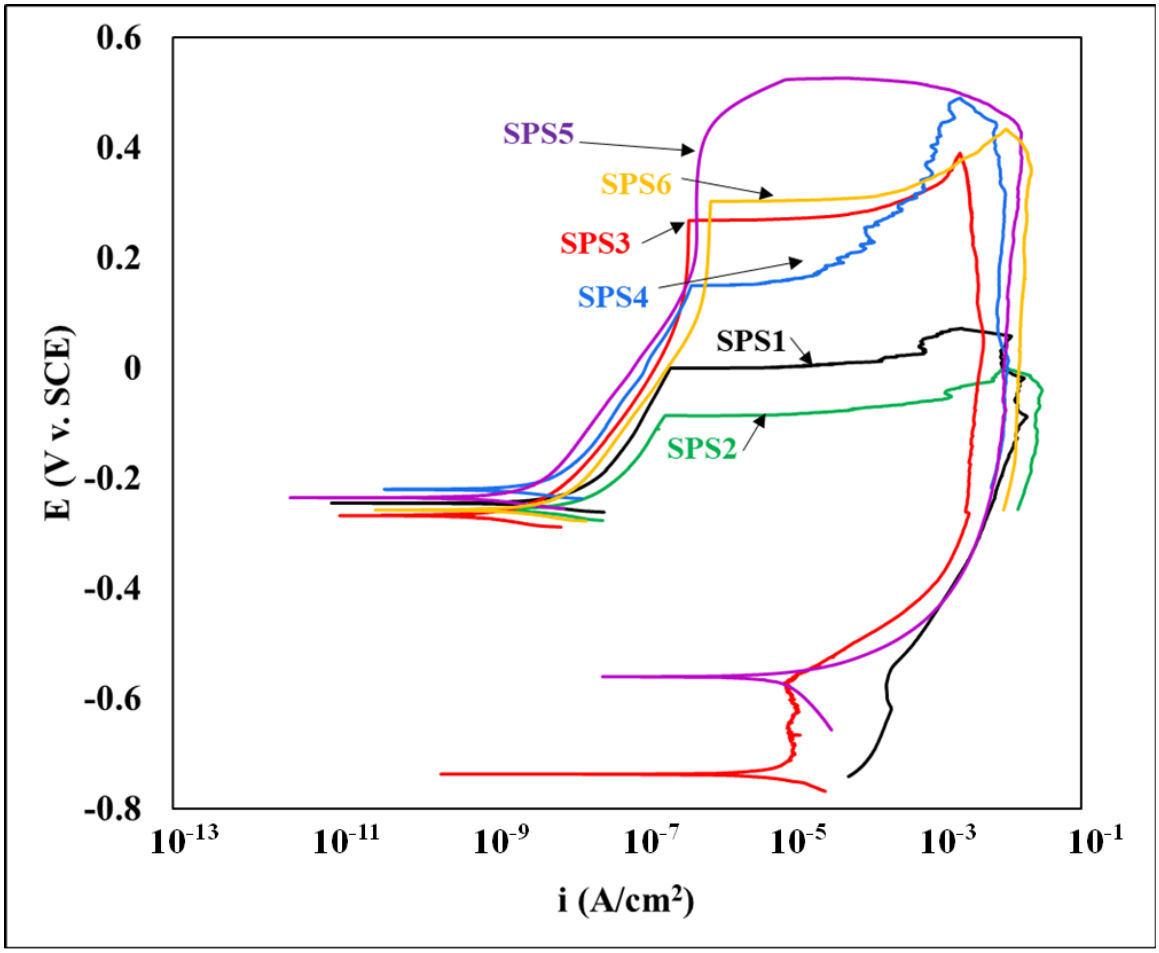

Figure 17. Anodic cyclical potentiodynamic polarization tests in SPS solutions containing 2 M Cl (SPS1 = SPS, SPS2 = SPS + 100 mL NMP, SPS3 = SPS + 400 mL NMP, SPS4 = SPS + 1 mM BPT + 100 mL NMP, SPS5 = SPS + 2 mM BPT + 200 mL NMP, SPS6 = SPS + 3 mM BPT + 300 mL NMP)

5.2.2. Preliminary Results

Results of the compressive and flow table tests are presented in Table 8. Due to the imprecise nature of the load frame used for the preliminary testing (load rate controlled by a valve) several specimens were improperly loaded and lost. These specimens are highlighted in red in the table. Nevertheless, a trend based on single values for each condition showed decreasing strength with conditions containing NMP. The results of the flow table tests showed decreased flow percentage with the addition of NMP, where it possibly affected the w/c ratio, and in turn the workability, of the mix as a reduction of water was needed to keep a consistent liquid volume. This is the case with BPT + NMP 1 condition, where the total liquid volume used in the specimens was exceeded since the total NMP volume was added to the total water volume and this increased the flow percentage. A leaching test performed using high performance liquid chromatography (HPLC) was performed and found no BPT or NMP in the curing water samples tested. Using this

knowledge, the mortar specimens produced for the further physico-mechanical and electrochemical tests were able to be mixed and prepared appropriately, allowing a more efficient use of material and proper preparation.

Table 8. Preliminary mortar specimen compression and slump test results

	Compressive Strength (MPa)				
Mortar Specimen	Measurement 1	Measurement 2	Measurement 3	AVG	Flow (%)
Control 1	36.2	29.0	11.8	29.0	N/A
Control 2	N/A	13.9	N/A	13.9	76.3
BPT	32.4	16.4	24.2	24.3	131.6
BPT + NMP 1	12.6	11.8	12.1	12.1	136.8
BPT + NMP 2	6.5	16.0	14.6	15.3	71.1

5.2.3. Mortar Specimens- BPT and Hybrid BPT/GP Effect

5.2.3.1. Physical-Mechanical Characterization of the Mortar

Compression Testing. Figure 18 shows the results of the compressive resistance, after 31 days of curing. As expected from the design, the compression resistance of the mortar is low and it is comparable to other concrete specimens of the same w/c ratio (72). The 2.5mM BPT concentration (added with the cement), showed the best compression resistance out of all the conditions tested. The specimens prepared with NMP showed the worst compression resistance. The GP mortar cubes, at both 0.45 and 0.65 w/c, showed similar values, both above the control condition. However, during the test, once the ultimate strength was achieved, the GP cubes had a very brittle failure mode, destroying the outer layers of the cube. This is in contrast with the OCP mortar specimens, which failed alongside the exposed face (the face of the cube not placed against a wall of the mold). This leads to a concern with the GP specimens where delamination of the cover can occur once a sufficient load is reached. Images after failure of an OPC mortar cube and a GP mortar cube can be seen in Figure 19.

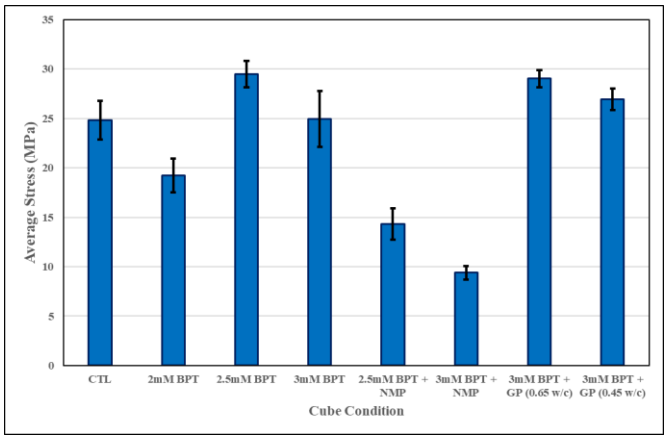

Figure 18. Mortar cube compression test results after 31 days of curing

a) OPC mortar specimen

b) GP mortar specimen

Figure 19. Mortar specimen after compressive testing

Resistivity Testing. The results of the resistivity tests following the DURAR manual (67) are seen in Figure 20. Once the electrical resistance, Re, was determined, the electrical resistivity is given by equation [3]:

$$p = R_e\,(A/L)\ (\text{ohm.cm}) \qquad [3]$$

The same trend was found when the resistivity was measured in the different specimens, after curing (31 days) and after evaluating the effective porosity of the mortar (36 days). As with the compression tests, the 2.5mM BPT displayed the best results (highest compressive strength). The inclusion of BPT increased the resistivity of the specimens, which indicates a less aggressive mortar for the reinforcement.

Porosity Testing. The results of the 31-day capillary absorption tests following the DURAR manual are shown in Figure 21. The capillary absorption test concerns the interconnectedness of the capillary pores present in the mortar or concrete as these pores affect the strength and accessibility of water or corrosive species (durability) to the rebar. The conditions show similar results for 0.65 w/c concrete specimens (72), although they showed lower water absorption. This is possibly due to the different aggregates size in the concrete, creating larger voids, while the mortar specimens use a more homogeneous aggregate, leading to smaller pores. In principle pastes and mortars should be more compact when compared to concrete due to the formation of the Interfacial Transition Zone (ITZ) at the interface with the larger aggregate particles of concrete. Therefore, the permeability of concrete should consequently be higher than that for mortar specimens. The NMP conditions show a clearer linear region compared to the non-NMP conditions (Figure 21), showing a significantly higher absorption rate.

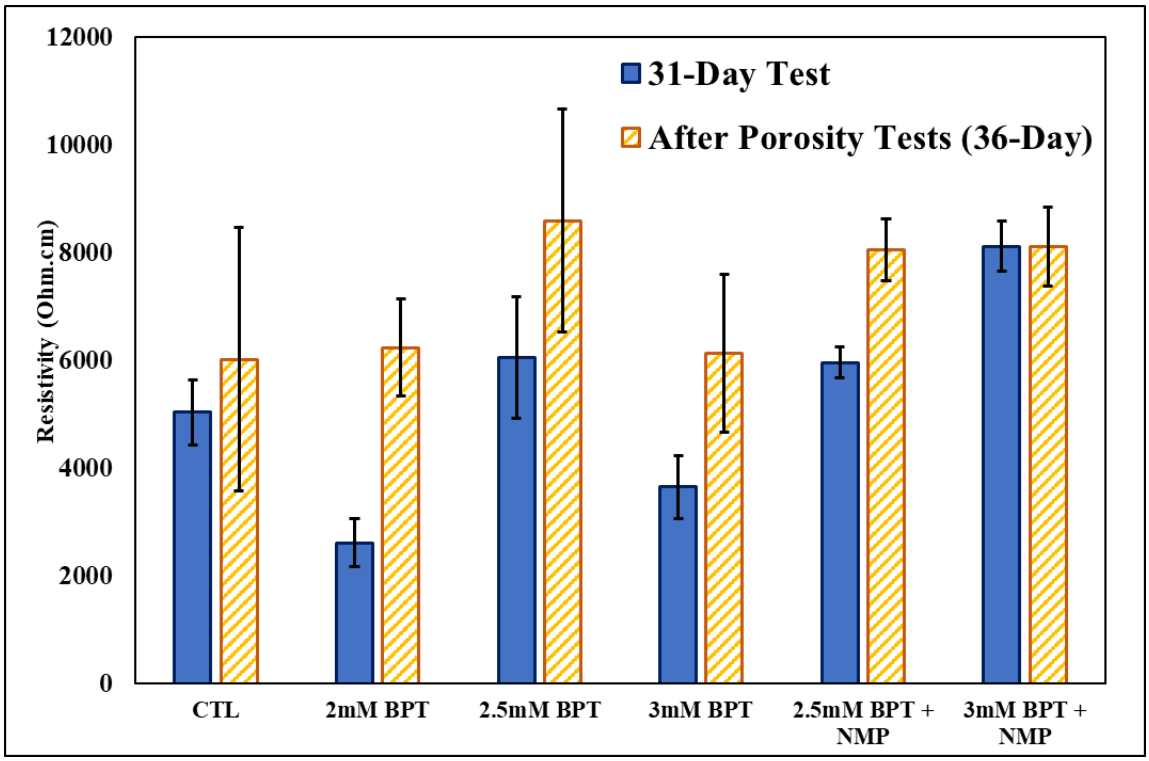

Figure 20. Mortar specimen resistivity tests, after 31 days of curing and after the water absorption test (36 days).

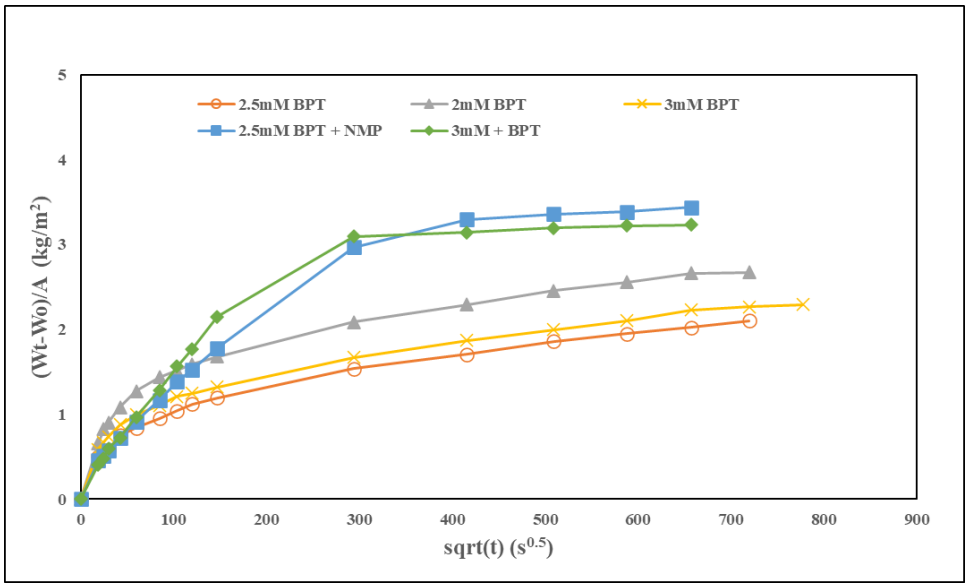

Figure 21. Mortar specimen 31 day capillary absorption tests

The method produces three coefficients: the mortar specimen's resistance to water penetration, m, the capillary absorption coefficient, k, and the effective porosity, εe (67). These are used to describe the kinetics of mortar capillary absorption and are calculated using the following formulas:

Resistance to water penetration

$$m = \frac{t}{z^2}\ (\mathrm{s/m^2})$$

Capillary absorption coefficient

$$k = \frac{(Wt - Wo)/A}{\sqrt{t}}\ (\mathrm{kg/m^2 s^{\frac{1}{2}}})$$

Effective porosity

$$\varepsilon_e = \frac{k\sqrt{m}}{10}\ (\%)$$

The coefficients Wt and Wo represent the weight value taken at the time of weighing and prior to the immersion of the specimen into the water tub, respectively. The dimensional qualities of the specimen were taken as area, A = 7.85x10-3 m2 and height, z = 0.03488 ± 0.002 m2. The coefficient k was calculated from the measurements recorded in the first 6 h measurement intervals. The values produced by these equations are used to calculate another coefficient, S, which is the capillary sorption coefficient, and is given by:

$$S = \frac{1}{\sqrt{m}}\ (\mathrm{m/s^{\frac{1}{2}}})$$

Both the S and εe coefficients are presented in Figure 22.

The results showed that, again, that 2.5 mM BPT, without NMP, improved the quality of the specimen from the point of view of durability, which is represented by a decrease in the average capillary sorption and effective porosity of the mortar. It is important to note that there is no statistically difference between the parameters for 2.5 mM BPT and 3 mM BPT.

When comparing all the physical-mechanical properties of the different mortars evaluated, it can be indicated that 2.5 mM BPT appears to be an optimal concentration in the mortar/concrete since there is no detrimental effect on these properties. However, it is necessary to perform another evaluation after 90 days of curing to determine the behavior of the NMP in the long term.

Regarding the hybrid corrosion control system (BPT + GP), it is also necessary to wait until the 90-days of curing to have the results of water absorption tests; but the compression resistance increased after 31-days of curing.

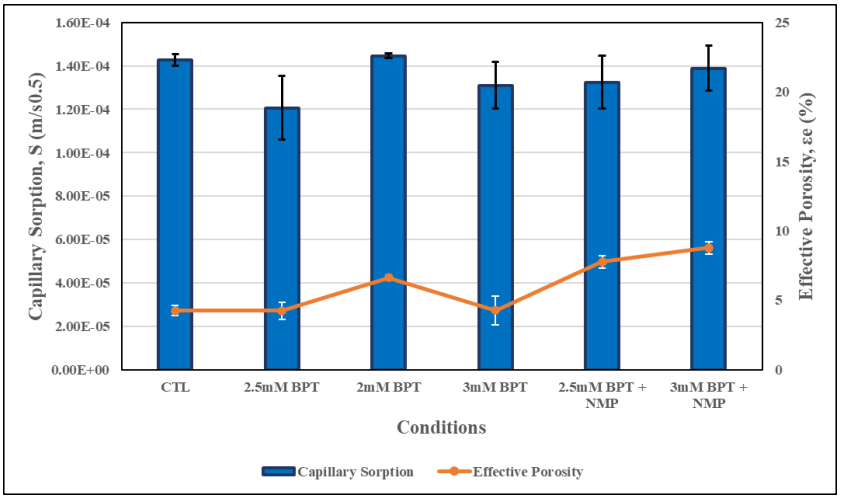

Figure 22. Mortar specimen capillary absorption tests at 31 days

5.2.3.2. Electrochemical Testing

The electrochemical tests performed up to date on samples sprays with salt following the modified ISP 11474 standard show promising results. After 20 days of exposure, results of the OCP measurements have shown values becoming more noble over time (Figure 23), showing the passivation of the embedded reinforcement as the specimen cured overtime. Initial Rp measurements of specimens containing only BPT, where they increase over time, more than the control and BPT + NMP counterparts (Figure 24).

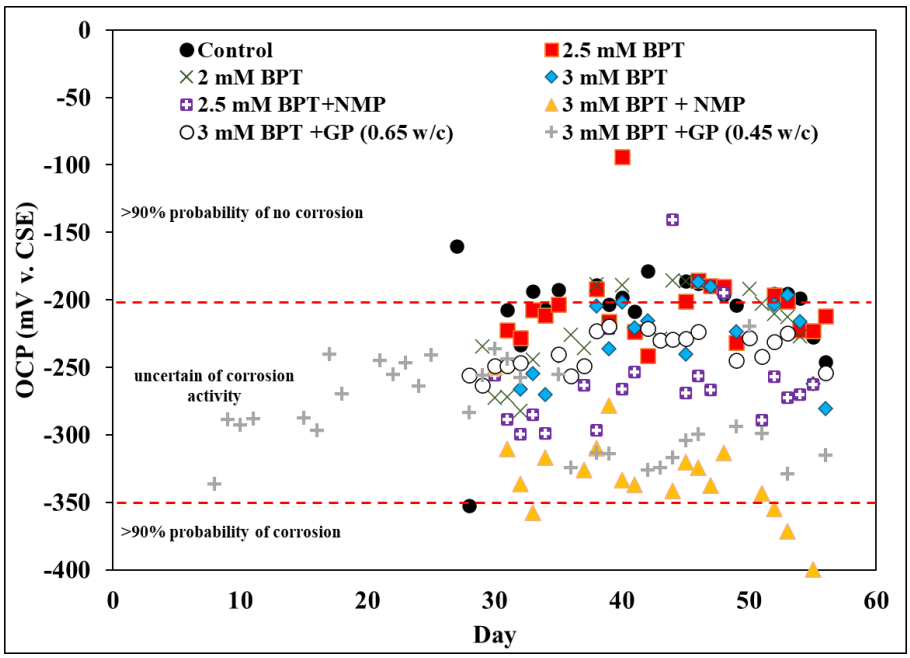

a) Rebar A

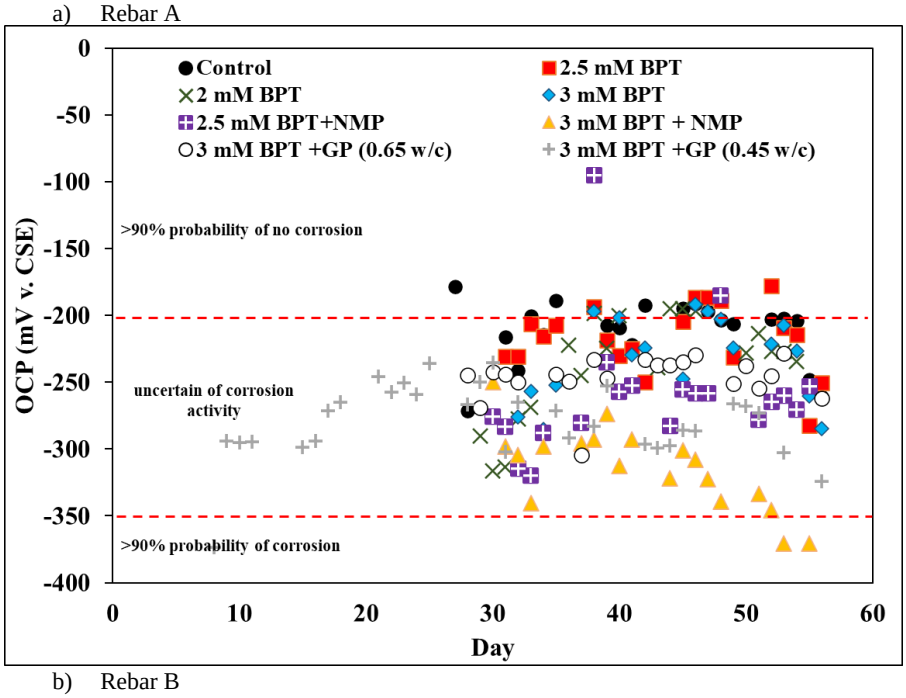

b) Rebar B

Figure 23. Mortar specimen OCP measurements during ISO11474 exposure

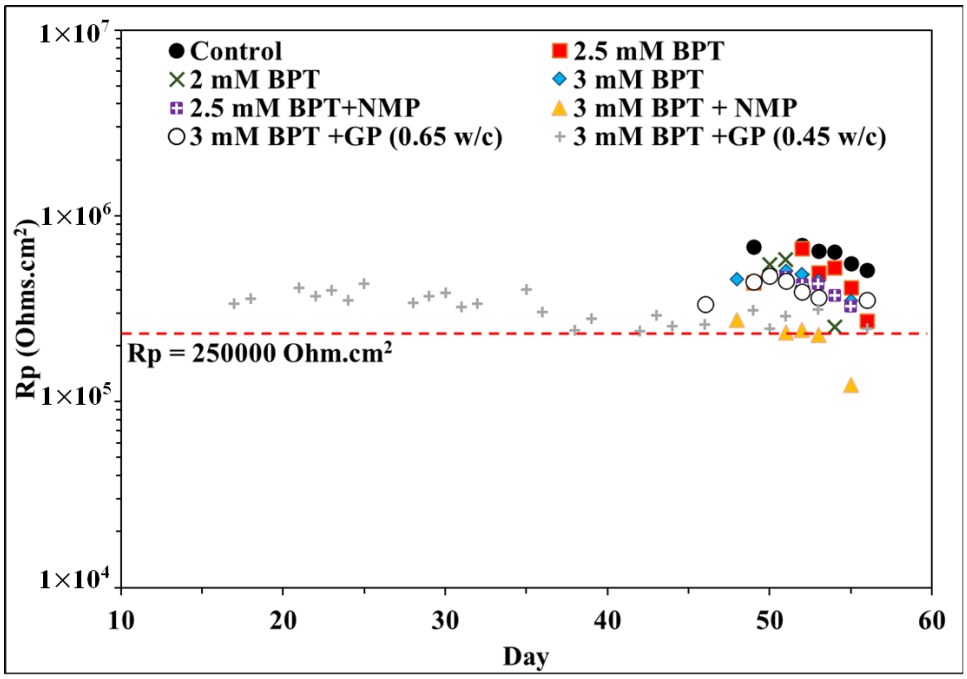

a) Rebar A

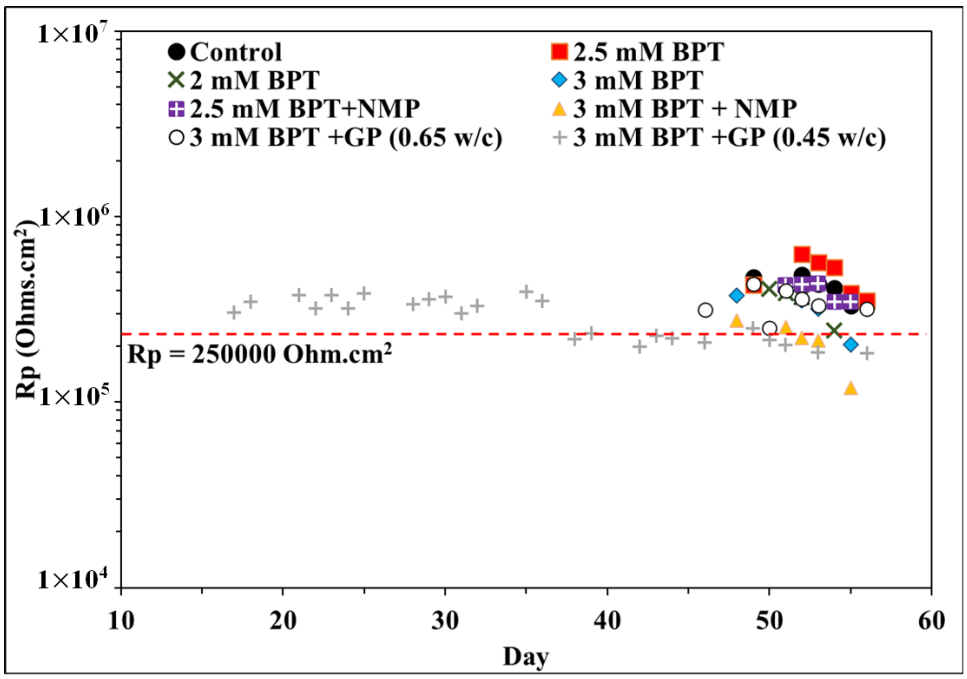

b) Rebar B

Figure 24. Mortar specimen Rp measurements during ISO11474 exposure

6. CONCLUSIONS

The durability of reinforced Geopolymer-based Concrete in the corrosive environment has been characterized with promising results from the mass transport process mechanism or physical barrier blocking mechanism.

The electrochemical results suggest physical barrier mechanism blocking the chloride when the GPC materials are formed, where the mass transport process dominates and the physical results. Overall, the potassium-based geopolymer could have protected the reinforcing steel from corrosion for over 60 days when the sample is exposed to the high concentration of chloride containing electrolytes.

With the presence of BPT and NMP as co-dissolver, it was found that their presence can help with enhancing the anti-corrosion property of the reinforcing steel according to the experiments with the simulated pore solution. The optical BPT concentration was found in between 2 to 2.5 mM for the best anti-corrosion performance. The physical-mechanical testing results are also indicative that the BPT can potentially be beneficial for the mortar's mechanical properties. However, the presence of NMP decreased such mechanical properties which may owing to the increased w/c ratio of the mortar system. Additionally, relatively higher mortar matrix porosity values were observed from the NMP-containing samples, which can negatively affect the barrier performance of the mortar matrix.

It was also found that the presence of chloride ions can decrease the inhibition efficiency according to both the polarization resistance range and calculated corrosion rate. According to the corrosion testings of the reinforced mortar samples following ISO11474, considerably higher anti-corrosion performance was observed in both 2 and 2.5mM BPT samples, and such substrate protection was prolonged over 50 days of immersion period. Meanwhile, it was also found that the higher BPT and NMP concentrations are not necessarily beneficial for the inhibiting performance, as the higher concentration of such compounds tended to decrease the barrier performance.

REFERENCES

1. Troconis de Rincon, O. Uso de los Inhibidores para el Control de la Corrosión del Acero de Refuerzo del Concreto. Presented at VIII Reunión Latinoamericana de Electroquímica y Corrosión, Barcelona, Argentina, 1988: pp. 444-446.

2. Martínez de Fernandez, N., y O. Troconis de Rincon. Efecto de los Inhibidores ZnO y $Ca(NO_2)_2$ y del Agua del Lago en las Propiedades Físico-químicas del Concreto. Presented at II Congreso Iberoamericano de Corrosión y Protección, , Maracaibo, Venezuela, 1986: pp. 397-403.

3. Bryan, N.S., D.D. Alexander, J.R. Coughlin, A.L. Milkowski and P. Boffetta. Ingested Nitrate and Nitrite and Stomach Cancer Risk: an Updated Review. Food and Chemical Toxicology, 2012. 50: 3646-3665.

4. Berke, N.S., M. Dallaire, M. Hicks and R. Hoopes. Corrosion of Steel in Cracked Concrete. Corrosion, 1993. 49: 934-943.

5. Troconis de Rincon, O., O. Perez, E. Paredes, Y. Caldera, C. Urdaneta and I. Sandoval. Long-term Performance of ZnO as a Rebar Corrosion Inhibitor. Cement and Concrete Composites, 2002. 24: 79-87.

6. Perez, O. Estudio del ZnO, $Ca(NO_2)_2$ y del $Ca_5(PO_4)_3OH$, como Inhibidores de Corrosión del Acero de Refuerzo en Concreto Preparado con Agua del Lago de Maracaibo. Master Thesis, 1993. Universidad del Zulia, Maracaibo, Venezuela.

7. Caldera Y. Estudio de la Calidad del Concreto sobre el Efecto Inhibidor del ZnO en el Acero de Refuerzo. Master Thesis, 1996. Universidad del Zulia, Maracaibo, Venezuela.

8. Sandoval, I. C., Urdaneta. Estudio de la Relación Agua/Cemento en el Comportamiento del ZnO y $Ca(NO_2)_2$ como Inhibidores de Armaduras. Thesis to get the Chemical Engineering degree, 1997. Universidad del Zulia, Maracaibo, Venezuela,

9. Troconis de Rincon, O., O. Perez, E. Paredes, Y. Caldera, C. Urdaneta and I. Sandoval. Long- term Performance of ZnO as Rebar Corrosion Inhibitor. Cement and Concrete Composites, 2002. 24: 79-87.

10. Ramirez, E. Corrosión de las Armaduras Embebidas en Hormigón en Ambientes de Extrema Agresividad. Posibilidad de Protección Mediante Inhibidores. PhD Thesis, 1994. Facultad de Ciencias Químicas, Universidad Complutense de Madrid, Madrid, España.

11. B.D. Prowell, The evaluation of corrosion inhibitors for the repair and rehabilitation of reinforced concrete bridge components, in, Virginia Tech, 1992.

12. M.L. Sousa Rivetti, J.d.S. Andrade Neto, N.S. de Amorim Júnior, D. Véras Ribeiro, Corrosion Inhibitors for Reinforced Concrete, in: Corrosion Inhibitors, Principles and Recent Applications, IntechOpen, 2017.

13. H.-S. Lee, V. Saraswathy, S.-J. Kwon, S. Karthick, Corrosion Inhibitors for Reinforced Concrete: A Review, in: Corrosion Inhibitors, Principles and Recent Applications, IntechOpen, 2017.

14. J.L. Bell, P.E. Driemeyer, W.M. Kriven, Formation of Ceramics from Metakaolin-Based Geopolymers. Part II: K-Based Geopolymer, Journal of the American Ceramic Society, 92 (2009) 607-615.
15. P. Duxson, A. Fernandez-Jimenez, J.L. Provis, G.C. Lukey, A. Palomo, J.S.J. van Deventer, Geopolymer technology: the current state of the art, J. Mater. Sci., 42 (2007) 2917-2933.

16. J.L. Provis, J.S.J. Van Deventer, Geopolymers: structures, processing, properties and industrial applications, Elsevier, 2009.
17. J. Davidovits, Geopolymer, Green Chemistry and Sustainable Development Solutions: Proceedings of the World Congress Geopolymer 2005, Geopolymer Institute, 2005.

18. M. Hussain, R.J. Varley, Y.B. Cheng, G.P. Simon, Investigation of thermal and fire performance of novel hybrid geopolymer composites, J. Mater. Sci., 39 (2004) 4721-4726.
19. T.W. Cheng, J.P. Chiu, Fire-resistant geopolymer produced by granulated blast furnace slag, Miner. Eng., 16 (2003) 205-210.

20. J.G.S. Van Jaarsveld, J.S.J. Van Deventer, A. Schwartzman, The potential use of geopolymeric materials to immobilise toxic metals: Part II. Material and leaching characteristics, Miner. Eng., 12 (1999) 75-91.
21. J. Temuujin, W. Rickard, M. Lee, A. van Riessen, Preparation and thermal properties of fire resistant metakaolin-based geopolymer-type coatings, Journal of Non-Crystalline Solids, 357 (2011) 1399-1404.

22. Hardjito, D., S. E. Wallah, D. M. Sumajouw, and B. V. Rangan. On the development of fly ash-based geopolymer concrete. *Materials Journal,* 2004. 101, 6: 467-472.

23. Hardjito, D., S. E. Wallah, D. M. J. Sumajouw, and B. V. Rangan. Factors Influencing the Compressive Strength of Fly Ash-Based Geopolymer Concrete. *Civil Engineering Dimension,* 2004. 6: pp. 88-93.
24. Hardjito, D., S. Wallah, D. Sumajouw, and B. Rangan. Introducing fly ash-based geopolymer concrete: manufacture and engineering properties.In *30th conference on our world in concrete & structures*, 2005: 23-24.

25. Shayan, A. Specification and use of geopolymer concrete in the manufacture of structural and non-structural components: review of literature.In, 2016.

26. Duxson, P., G. C. Lukey, and J. S. J. van Deventer. Physical evolution of Na-geopolymer derived from metakaolin up to 1000 °C. *Journal of Materials Science,* 2007. 42: 3044-3054.

27. Mo, B.-h., H. Zhu, X.-m. Cui, Y. He, and S.-y. Gong. Effect of curing temperature on geopolymerization of metakaolin-based geopolymers. *Applied Clay Science,* 2014. 99: 144-148.

28. White, C. E., J. L. Provis, T. Proffen, and J. S. Van Deventer. The effects of temperature on the local structure of metakaolin-based geopolymer binder: A neutron pair distribution function investigation. *Journal of the American Ceramic Society,* 2010. 93, 10: 3486-3492.

29. Zhang, B., K. J. MacKenzie, and I. W. Brown. Crystalline phase formation in metakaolinite geopolymers activated with NaOH and sodium silicate. *Journal of Materials Science,* 2009. 44, 17: 4668-4676.

30. Bell, J. L., P. E. Driemeyer, and W. M. Kriven. Formation of ceramics from metakaolin-based geopolymers. Part II: K-based geopolymer. *Journal of the American Ceramic Society,* 2009. 92, 3: 607-615.

31. Duxson, P., J. L. Provis, G. C. Lukey, F. Separovic, and J. S. van Deventer. 29Si NMR study of structural ordering in aluminosilicate geopolymer gels. *Langmuir,* 2005. 21, 7: 3028-3036.

32. Lizcano, M., H. S. Kim, S. Basu, and M. Radovic. Mechanical properties of sodium and potassium activated metakaolin-based geopolymers. *Journal of Materials Science,* 2012. 47: 2607-2616.

33. Rowles, M., and B. O'Connor. Chemical optimisation of the compressive strength of aluminosilicate geopolymers synthesised by sodium silicate activation of metakaolinite. *Journal of Materials Chemistry,* 2003. 13, 5: 1161-1165.

34. Zhang, M., M. Zhao, G. Zhang, T. El-Korchi, and M. Tao. A multiscale investigation of reaction kinetics, phase formation, and mechanical properties of metakaolin geopolymers. *Cement and Concrete Composites,* 2017. 78: 21-32.

35. Subaer, and A. van Riessen. Thermo-mechanical and microstructural characterisation of sodium-poly(sialate-siloxo) (Na-PSS) geopolymers. *Journal of Materials Science,* 2007. 42, 9: 3117-3123.

36. Marín-López, C., J. L. Reyes Araiza, A. Manzano-Ramírez, J. C. Rubio Avalos, J. J. Perez-Bueno, M. S. Muñiz-Villareal, E. Ventura-Ramos, and Y. Vorobiev. Synthesis and characterization of a concrete based on metakaolin geopolymer. *Inorganic Materials,* 2009. 45, 12: 1429-1432.

37. Olivia, M., and H. Nikraz. Properties of fly ash geopolymer concrete designed by Taguchi method. *Materials & Design (1980-2015),* 2012. 36: 191-198.

38. Škvára, F., V. Šmilauer, P. Hlaváček, L. Kopecký, and Z. Cílová. A weak alkali bond in (N, K)-A-S-H gels: Evidence from leaching and modeling. *Ceramics - Silikaty,* 2012. 56: 374-382.

39. Mehta, P. K., and P. J. Monteiro. *Concrete microstructure, properties and materials*. McGraw-Hill Education, 2017.

40. Provis, J. L., and J. S. J. Van Deventer. *Geopolymers: structures, processing, properties and industrial applications*. Elsevier, 2009.

41. Davidovits, J. *Geopolymer, green chemistry and sustainable development solutions: proceedings of the world congress geopolymer 2005*. Geopolymer Institute, 2005.

42. Miranda, J. M., A. Fernández-Jiménez, J. A. González, and A. Palomo. Corrosion resistance in activated fly ash mortars. *Cement and Concrete Research,* 2005. 35: 1210-1217.

43. Reddy, D. V., J.-B. Edouard, and K. Sobhan. Durability of Fly Ash–Based Geopolymer Structural Concrete in the Marine Environment. *Journal of Materials in Civil Engineering,* 2013. 25: 781-787.

44. Shaikh, F. U. A. Effects of alkali solutions on corrosion durability of geopolymer concrete. 2014. 2: 109-123.

45. Chindaprasirt, P., and W. Chalee. Effect of sodium hydroxide concentration on chloride penetration and steel corrosion of fly ash-based geopolymer concrete under marine site. *Construction and Building Materials,* 2014. 63: 303-310.

46. Babaee, M., and A. Castel. Chloride-induced corrosion of reinforcement in low-calcium fly ash-based geopolymer concrete. *Cement and Concrete Research,* 2016. 88: 96-107.

47. Tennakoon, C., A. Shayan, J. G. Sanjayan, and A. Xu. Chloride ingress and steel corrosion in geopolymer concrete based on long term tests. *Materials & Design,* 2017. 116: 287-299.

48. Gunasekara, C., D. Law, S. Bhuiyan, S. Setunge, and L. Ward. Chloride induced corrosion in different fly ash based geopolymer concretes. *Construction and Building Materials,* 2019. 200: 502-513.

49. Zhang, R., A. Castel, and R. François. Influence of steel–concrete interface defects owing to the top-bar effect on the chloride-induced corrosion of reinforcement. *Magazine of concrete research,* 2011. 63, 10: 773-781.

50. ACI Committee 211. (1991). Standard Practice for Selecting Proportions for Normal, Heavyweight, and Mass Concrete (ACI 211.1-91) (Reapproved 2002). Farmington Hills, MI :American Concrete Institute.

51. Ahmed Elshami, Stéphanie Bonnet, Abdelhafid Khelidj and Latefa Sail (2020). Effectiveness of corrosion inhibitors in simulated concrete pore solution, European Journal of Environmental and Civil Engineering, 24:13.

52. Jones, D. A. (1996). Principles and prevention of corrosion (2nd ed.). Prentice Hall.

53. N.S. Berke, M. Dallaire, M. Hicks, R. Hoopes, Corrosion of steel in cracked concrete, Corrosion, 49 (1993) 934-943.

54. N.S. Bryan, D.D. Alexander, J.R. Coughlin, A.L. Milkowski, P. Boffetta, Ingested nitrate and nitrite and stomach cancer risk: an updated review, Food and Chemical Toxicology, 50 (2012) 3646-3665.

55. C. M. Fernandes, L. X. Alvarez, N. Escarpini dos Santos, A. C. Maldonado Barrios, E. A. Ponzio, Corros. Sci. 149 (2019), 185-194.

56. Asipita SA, Ismail M, Majid MZA, Majid ZA, Abdullah C, Mirza J. Green bambusa arundinacea leaves extract as a sustainable corrosion inhibitor in steel reinforced concrete. Journal of Cleaner Production. 2014;67(15):139-146.

57. L. K. M. O Goni and M. A. J. Mazumder. Green Corrosion Inhibitors, in: Corrosion Inhibitors, IntechOpen, 2019.

58. ASTM Standard C33, 2018, "Specification for Concrete Aggregates," ASTM International, West Conshohocken, PA, 2018, DOI: 10.1520/C0033_C0033M-18, www.astm.org.

59. ASTM Standard C778, 2017, "Specification for Standard Sand," ASTM International, West Conshohocken, PA, 2017, DOI: 10.1520/C0778-17, www.astm.org.

60. ASTM Standard C876, 2015, "Corrosion Potentials of Uncoated Reinforcing Steel in Concrete," ASTM International, West Conshohocken, PA, 2015, DOI: 10.1520/C0876-15, www.astm.org.

61. ASTM Standard G59, 1997 (2020), "Standard Test Method for Conducting Potentiodynamic Polarization Resistance Measurements," ASTM International, West Conshohocken, PA, 2020, DOI: 10.1520/G0059-97R20, www.astm.org.

62. International Organization for Standardization. 1998 (2019). Corrosion of metals and alloys – Corrosion tests in artificial atmosphere – Accelerated outdoor test by intermittent spraying of a salt solution (Scab test) (ISO Standard No. 11474:2019). https://www.iso.org/standard/19426.html

63. ASTM Standard C109, 2021, "Standard Test Method for Compressive Strength of Hydraulic Cement Mortars (Using 2-in. or [50 mm] Cube Specimens)," ASTM International, West Conshohocken, PA, 2021, DOI: 10.1520/C0109_C0109M-21, www.astm.org.

64. ASTM C1437 ASTM Standard C1437, 2020, "Standard Test Method for Flow of Hydraulic Cement Mortar," ASTM International, West Conshohocken, PA, 2020, DOI: 10.1520/C1437-20, www.astm.org.

65. ASTM Standard C230, 2021, "Standard Specification for Flow Table for Use in Tests of Hydraulic Cement," ASTM International, West Conshohocken, PA, 2021, DOI: 10.1520/C0230_C230M-21, www.astm.org.

66. Hornbostel, K., Larsen, C.K., and Geiker, M.R. (2013). Relationship between concrete resistivity and corrosion rate – A literature review. Cement & Concrete Composites. 39 (2013) 60-72

67. O. Troconis de Rincon and DURAR Network Members, Manual for Inspecting, Evaluating and Diagnosing Corrosion in Reinforced Concrete Structures. CYTED. ISBN 980-296-541-3 Maracaibo, Venezuela. 2000 (1st Edition in English).

68. Ford, S., J. Shane, and T. O. Mason. Assignment of features in impedance spectra of the cement-paste/steel system. *Cement and Concrete Research*, 1998. 28, 12: 1737-1751.

69. Hirschorn, B., M. E. Orazem, B. Tribollet, V. Vivier, I. Frateur, and M. Musiani. Constant-phase-element behavior caused by resistivity distributions in films: I. Theory. *Journal of The Electrochemical Society*, 2010. 157, 12: C452.

70. Hsu, C., and F. Mansfeld. Concerning the conversion of the constant phase element parameter Y0 into a capacitance. *Corrosion*, 2001. 57, 9: 747-748.

71. ASTM Standard G102, 1989 (2015), "Standard Practice for Calculation of Corrosion Rates and Related Information from Electrochemical Measurements," ASTM International, West Conshohocken, PA, 2015, DOI: 10.1520/G0102-89R15E01, www.astm.org.

72. Rincon, O.T. and Duracon Collaboration. (2005). Durability of concrete structures: DURACON, an iberoamerican project. Preliminary results. Building and Environment. 41 (2006). 952-962.